How to cite: *Angew. Chem. Int. Ed.* **2025**, *64*, e202415071
doi.org/10.1002/anie.202415071

Nanographene Electrocatalysts

Structural Modulation of Nanographenes Enabled by Defects, Size and Doping for Oxygen Reduction Reaction

Bin Wu[#+], Haibing Meng[#], Xingbao Chen[#], Ying Guo, Li Jiang, Xiaofeng Shi, Jiexin Zhu,* Juncai Long, Wenliang Gao, Feng Zeng, Wen-Jie Jiang,* Yongfa Zhu, Dingsheng Wang, and Liqiang Mai**

Abstract: Nanographenes are among the fastest-growing materials used for the oxygen reduction reaction (ORR) thanks to their low cost, environmental friendliness, excellent electrical conductivity, and scalable synthesis. The perspective of replacing precious metal-based electrocatalysts with functionalized graphene is highly desirable for reducing costs in energy conversion and storage systems. Generally, the enhanced ORR activity of the nanographenes is typically deemed to originate from the heteroatom doping effect, size effect, defects effect, and/or their synergistic effect. All these factors can efficiently modify the charge distribution on the sp^2-conjugated carbon framework, bringing about optimized intermediate adsorption and accelerated electron transfer steps during ORR. In this review, the fundamental chemical and physical properties of nanographenes are first discussed about ORR applications. Afterward, the role of doping, size, defects, and their combined influence in boosting nanographenes' ORR performance is introduced. Finally, significant challenges and essential perspectives of nanographenes as advanced ORR electrocatalysts are highlighted.

1. Introduction

Since the beginning of the 21st century, issues such as resource depletion, environmental pollution, and the greenhouse effect, all exacerbated by the massive utilization of fossil fuels, have become increasingly critical. The traditional energy structure needs to be revised to meet the growing needs for sustainable development and human survival.[1–4] Therefore, it is clear that the global energy issues call for transformative clean technologies that should be be sustainable, environmentally friendly, efficient, and affordable.[5] Electrochemical energy conversion technologies, such as polymer electrolyte membrane fuel cells (PEMFCs) and metal–air batteries (MABs) have shown significant potential to meet these requirements, offering a pathway toward a new era of green energy.[3, 5–6]

The electrochemical oxygen reduction reaction (ORR) is a key process in energy conversion applications, including PEMFCs, MABs, and H_2O_2 production.[7–11] In aqueous electrolytes, ORR is generally regarded as the efficiency-determining process in those energy devices and proceeds through two primary pathways: the 4-electron reduction of

[*] Dr. B. Wu[# +]
Helmholtz-Zentrum Berlin für Materialien und Energie GmbH, Albert-Einstein-Straße 15, 12489 Berlin, Germany
Dr. B. Wu[# +]
Institute of Physics, Humboldt University Berlin, Newton-Straße 15, 12489 Berlin, Germany
Dr. H. Meng,[#] Y. Guo
College of Chemistry and Chemical Engineering, Taiyuan University of Technology, 030024 Taiyuan,
E-mail: menghaibing@tyut.edu.cn
X. Chen,[#] Dr. J. Zhu, J. Long, Prof. L. Mai
State Key Laboratory of Advanced Technology for Materials Synthesis and Processing, School of Materials Science and Engineering, Wuhan University of Technology, Luoshi Road 122, 430070 Wuhan, China
E-mail: jxzhu@whut.edu.cn
mlq518@whut.edu.cn
L. Jiang
CAS Key Laboratory of Molecular Nanostructure and Nanotechnology, CAS Research/Education Center for Excellence in Molecular Sciences, Institute of Chemistry, Chinese Academy of Sciences (CAS), 100190 Beijing, China
X. Shi
School of Environment and Safety Engineering, North University of China, 030051 Taiyuan, China
W. Gao
College of Chemistry and Chemical Engineering, Chongqing University, Chongqing 400044, China
F. Zeng
State Key Laboratory of Materials-Oriented Chemical Engineering, College of Chemical Engineering, Nanjing Tech University, 211816 Nanjing, China
Dr. W.-J. Jiang
Department of Chemical Engineering, The University of Melbourne, 3010 Melbourne, Victoria,
E-mail: wenjie.jiang@unimelb.edu.au
Y. Zhu, D. Wang
Department of Chemistry, Tsinghua University, 100084 Beijing, China
[#] Present address: School of Materials Science and Engineering, Nanyang Technological University, 50 Nanyang Avenue, Singapore 639798, Singapore
[+] These authors contributed equally to this work

O_2 to H_2O in acidic electrolytes or to OH^- in alkaline electrolytes, and the 2-electron reduction of O_2 to H_2O_2 in acidic electrolytes or to HO_2^- in alkaline electrolytes.[5, 12] However, the inherently low kinetics of the ORR limit the performance of these devices.[5] In past decades, platinum-based catalysts become the benchmark due to their relatively high ORR performance. However, their high cost and susceptibility to metal dissolution have spurred the search for alternative non-platinum materials that offer competitive activity, enhanced durability, and satisfactory cost.[13–14]

Among various non-platinum-based materials explored, a series of metal-free catalysts offer an eco-friendly alternative to traditional platinum-based catalysts, with materials like nanographenes,[15–16] fullerene,[17] carbon nanotubes,[18] black phosphorus[19] and borophene[20] proving highly effective. These catalysts exhibit excellent stability, conductivity, and selectivity while reducing costs and avoiding metal-related issues such as scarcity and toxicity.[21] Nanographenes is becoming a rising star in ORR catalysts due to its unique structure and tunable electronic properties compared to other ORR-based metal-free catalysts.[15] Unlike borophene and black phosphorus, facing stability challenges based on early investigations,[19–20] nanographenes exhibit remarkable chemical stability under harsh reaction conditions.[15] Meanwhile, nanographenes' 2D structure provides a higher density of active sites for ORR application than carbon nanotube and fullerene.[15] It is worth noting that nanographenes materials, particularly those synthesized from graphite, usually contain notable levels of metallic impurities that impact their electrochemical properties.[22] The use of metal oxidants or catalysts during the synthesis process inevitably introduces trace metals into nanographenes, playing an important role in overall catalytic performance.[22] Therefore, when claiming metal-free nanographenes, the determination of metallic impurities is very critical to identify whether the active center is only from the nanographenes matrix. Nanographenes, consisting of sp^2-hybri-

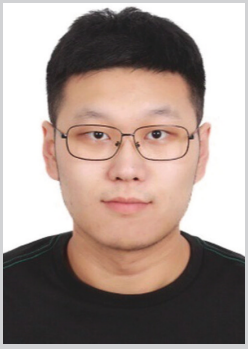

Bin Wu is a now a Postdoc Researcher in School of Materials Science and Engineering, Nanyang Technological University (Singapore). He obtained his Ph.D. degree from the Helmholtz-Zentrum Berlin für Materialien und Energie and Humboldt University of Berlin in 2023. He received his B.E. degree in Materials Chemistry from Chongqing University in China in 2016 as well as master degree in Materials Engineering from Institute of Chemistry, Chinese Academy of Sciences in 2019. His current research interests focus on in situ characterization of carbon nanomaterials for energy storage and conversion.

Haibing Meng received his Ph.D. in physical chemistry from Institute of Chemistry, Chinese Academy of Sciences, China (2019). From Sep. 2019 to Sep. 2021, he worked as a postdoctoral researcher in the Department of Chemical Engineering at Tsinghua University, China. Currently, he is an associate professor at the Taiyuan University of Technology, China. His research interests focus on the design and fabrication of nanomaterials for gas adsorption and separation, electrocatalysis, and photocatalysis.

Wen-Jie Jiang is a Fellow of the Australian Research Council's Discovery Early Career Researcher Award (DECRA) at the Department of Chemical Engineering, University of Melbourne. He earned his PhD in Physical Chemistry from the Institute of Chemistry, Chinese Academy of Sciences in 2017. His research centres on the design of electrocatalyst materials and the regulation of ion atmospheres at electrochemical interfaces, targeting efficient small molecule electrosynthesis while addressing critical challenges in ion transport, such as ion sieving, seawater deionisation, and sustainable recovery of valuable metals.

Jiexin Zhu received his Ph.D. (2023) in Materials science and Engineering at Wuhan University of Technology in Prof. Liqiang Mai's research group. Now, he is a postdoctoral fellow in the University of Toronto, co-supervised by Prof. David Sinton and Prof. Edward Sargent. His primary research lies in the field of electrocatalysis, with specific interests in CO_2/CO reduction, methanol oxidation, and oxygen evolution reactions. His work emphasizes the control of the surface coordination environment of electrocatalysts and employs in-situ characterization techniques, including infrared spectroscopy, Raman spectroscopy, and X-ray absorption spectroscopy.

Liqiang Mai is the Chair professor of Materials Science and Engineering at WUT, Dean of School of Materials Science and Engineering at WUT, Fellow of the Royal Society of Chemistry. He received his Ph.D. from WUT in 2004 and carried out his postdoctoral research at Georgia Institute of Technology in 2006–2007. He worked as an advanced research scholar at Harvard University and University of California, Berkeley. His current research interests focus on new nanomaterials for electrochemical energy storage and micro/nano energy devices.

dized carbon atoms settled in a hexagonal lattice, have attracted intensive attention as a promising candidate for ORR over the past decade. This is largely due to its excellent electrical conductivity, large surface area, and robust mechanical properties.[1, 6, 23] However, graphene's zero-band-gap property limits its catalytic activity.[3] Unmodified graphene shows relatively low electrocatalytic activity for ORR, making it unsuitable for direct use as a catalyst for PEMFCs and MABs.[3] A significant breakthrough in carbon-based electrocatalysts can be traced back to Dai's pioneering work on nitrogen-doped carbon nanotubes in 2009, which significantly enhanced catalytic performance.[1, 24] After that, many attempts have focused on modifying graphene by doping it with various heteroatoms (N, B, S, O, P, etc.) to create active sites that favor O_2 adsorption. These modifications have improved electrocatalytic performance due to their facile synthesis, excellent activity, and improved durability.[25–26] Accompanying the deepening insights into heteroatom doping effects, defective carbon nanomaterials without dopants also demonstrated considerable ORR activity since 2015, when the intrinsic carbon defects within the carbon framework were strategically regulated. These defects can be even superior to heteroatom-doped carbon electrocatalysts.[2, 27–28] Much research has evidenced that the existence of intrinsic carbon defects would have more or less impact on the whole charge state of the carbon matrix, thus increasing the density of active sites and lifting up the overall electrochemical performance of carbon nanomaterials.[2, 29] Given that a certain amount of disorder or defects are unavoidably formed in crystalline materials due to thermodynamics principles during the synthesis process and that these defects can be beneficial for electrocatalytic applications, many researchers have developed a series of non-doped defective nanographenes materials tailored to optimize ORR performance.[30–32] Furthermore, it is extensively recognized that the electronic structure of nanographenes is strongly dependent on the geometric size, which can change the electrocatalytic activity, exemplified by the quantum size effect.[33–35] Over the past decade, substantial efforts have been made to achieve controllable regulation of graphene size to tune electrocatalytic activity towards ORR.[33–34] In this regard, great advances have been made in material engineering and configuration investigations for nanographenes-based ORR catalysts.[2, 26] Since 2011, researchers have developed a class of functionalized nanographenes with tailored sizes, optimal doping, and controlled defectiveness to enhance ORR performance.[33–47]

Nevertheless, the basic knowledge of the vital active sites and catalytic mechanisms in functionalized graphene toward ORR needs to be clarified.[13] The exploration of the competition of active sites from different heteroatom configurations and dopant species (e.g., pyridinic N, pyrrolic N, graphitic N) is still urgently needed.[48] Moreover, the impact of the location of dopants in the matrix on electrochemical performance is still missing.[48] Beyond that, the controllable creation of defects in favor of enhanced ORR and understanding of reaction pathways triggered by defects and/or dopants remain missing.[48] Most importantly, the defects effect or/and size effect has a similar efficacy toward electrocatalytic ORR compared with heteroatom doping. However, in most cases, the ORR activity of the doped graphene materials is superior to that of non-doped defective graphene or small-size graphene.[49–51] As a whole, the resulting catalysts usually remarkably deliver the highest ORR activity when combining the defects or/and tuned size with suitable dopants, indicating that the defects or/and size and dopants can contribute together and synergistically promote the ORR activity for nanographenes.[2]

Recently, although the work of heteroatom-doped or defect-induced nanocarbon for ORR has been reviewed from the aspects of both materials design and structure analysis as shown in Figure 1,[2,7, 13–14] a few pieces of literature are systematically and comprehensively discussing some essential insights for targeted optimization of nanographenes, in particular, the impact on ORR via synergistic effect of heteroatom doping, size tailoring and defect inducing. More than that, the elaboration on critical active sites and intrinsic mechanisms based on enhanced performance towards ORR via doping effect, size effect and defects effect, especially their synergistic promotion by co-engineering. Therefore, in this review, we comprehensively summarize the progress of functionalized nanographenes via modifications of tuned dopants, tailored size and modulated defects toward ORR over the last decade. First, an introduction to the structure properties of nanographenes toward ORR, including the chemical structure and classifications of graphene is given. Then, representative studies highlighting modulations of nanographenes to enhance ORR performance by utilization of defects effect, size effect, doping effect, and their synergistic effect are summarized subsequently. Finally, an outlook of remaining challenges and potential perspectives on the doping effect, size effect, and defects effect, along with their synergy function toward ORR, is proposed at the end.

2. Structure Properties of Nanographenes for ORR

Since the first discovery of graphene by Geim and Novoselov in 2004, fast development of graphene-based materials has been promoted in the past two decades.[52] Among them, nanographenes deemed as a class of carbon materials with the whole or part of their dimensions being below 10 nm, such as graphene quantum dots (GQDs), graphene nanoribbons (GNRs), and three-dimensional graphenes (3D–Gs),[53–54] have garnered significant research attention due to their tunable and finite band gaps.[54] Especially, they have exhibited tremendous potential as ORR catalysts in PEMFCs and MABs owing to their abundant active sites, edge effects, and interconnection networks.[55] GQDs are typically quasi-0D nanographenes with three dimensions and sizes of less than 10 nm,[56] therefore, they are raising much research attention due to their fantastic optical and semiconductor properties.[56] GQDs usually are supported on the substrate due to the aggregation caused by their nanosized structures.[57] By assembling GQDs on the substrate, the electroneutrality of

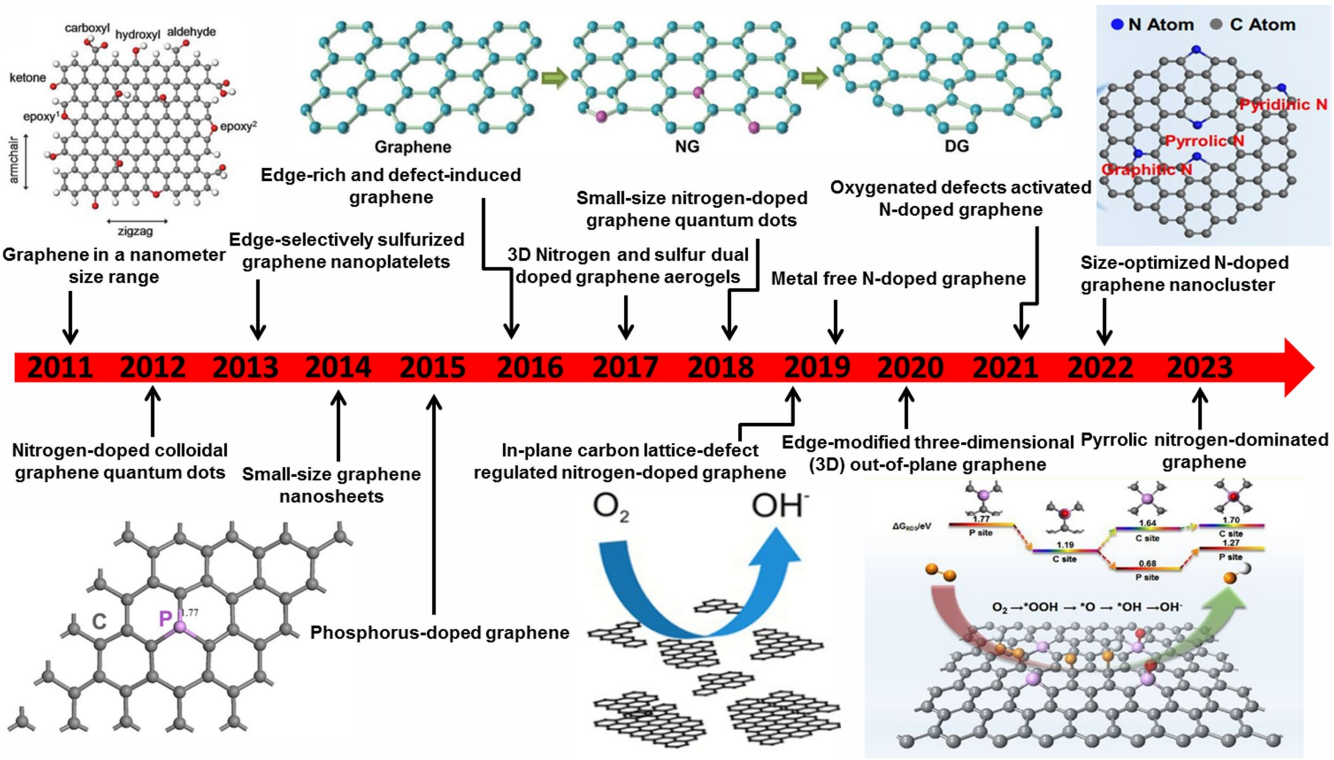

Figure 1. Timeline showing important developments of nanographenes-based ORR catalysts functionalized with various dopants, size and defects.

the substrate can be disrupted, generating new active centers for oxygen-containing intermediates desorption and adsorption, which can significantly improve the ORR performance. Additionally, the abundant edges of quantum dots can provide more catalytically active centers for ORR.[58] Moreover, GNRs are nanographenes with large aspect ratios (more than 10), which possess excellent mechanical, physical, and electrical properties, rendering them suitable alternatives for electrocatalysts.[59] The intrinsic size and high aspect ratio of GNRs result in their abundant exposed active edges, which promote the ORR activities by lowering potential barriers for electron transfer and oxygen-containing intermediates adsorption.[60] In addition, 3D–Gs are porous carbon materials linked by nanographene counterparts.[61] Their open 3D structure prevents the stacking and aggregation of graphene layers, creating an excellent conductive network. Additionally, 3D–Gs offer numerous active centers and facilitate fast ion diffusion and electron transfer during catalysis.[62] Based on the advantages of GQDs, GNRs, and 3D–Gs, much attention has been devoted to developing their ORR applications.[23]

For nanographenes, their electronic properties strongly depend on the influence of sizes and defects, which could induce edges that disrupt the infinite π-electron system. Therefore, the sizes and defects of nanographenes determine their chemical and physical properties and, ultimately, the ORR performance. For example, Tour et al. prepared graphene nanoribbons with jagged edges by treating multi-walled carbon nanotubes (CNTs) with H_2SO_4 and $KMnO_4$.[63] In particular, Shui et al. developed jagged edge GNRs (GNR@CNT) with CNT backbones and used them as metal-free ORR electrocatalysts for H_2/O_2 PEMFCs.[64] The carbon nanotube skeleton and carbon black spacer enhanced the mass transfer of the catalysts and the jagged carbon active sites at the GNR edges. Compared with Fe-N–C catalysts, GNR@CNTs exhibited higher stability in PEMFCs. This study demonstrates the great potential of defective graphitic carbon for PEMFCs application.

At a molecular level, nanographenes consist of layers of carbon atoms that are chemically bonded in the characteristic hexagonal pattern of graphite.[53] To pursue higher ORR performance, many atoms, such as oxygen, nitrogen, sulfur, et al., have been introduced into the skeleton of nanographene, namely doping.[65–66] Thus, many nanographenes with heteroatoms have been harvested, and the doping effects play an important role in boosting their ORR performance. For example, Li et al. successfully prepared a high-performance metal-free P, N-doped carbon porous foam catalyst (P–N-gfs-HMPA) with an $E_{1/2}$of about 0.78 V by using GO and carbon nanotubes as "building blocks" and hexamethylphosphoric acid triamide (HMPA) as a special precursor of P and N.[67] Based on the excellent porous structure and high electron transport capacity of graphene nanoparticles, as well as the high uptake of P and N from the HMPA compounds induced high density of coupled N–P groups, the foam exhibits an excellent electrocatalytic performance for ORR in acidic media. In particular, the ORR onset and half-wave potential reached 0.98 and 0.78 V in 0.1 M $HClO_4$, respectively, 50–100 mV higher than those of the previously reported metal-free carbon. Besides, the

more excellent nanographenes-based ORR catalysts have been obtained by considering the synergistic effects from defect, size, and doping.[68] Lu constructed a large number of in-plane nanopores with high oxygen content in graphene-based materials by acoustochemical etching of graphene oxide and sequential chemical reduction treatment, which effectively improved the electrochemical energy storage capacity and high output power density.[69] In addition, after the reduction of graphene oxide by hydrazine, porous substrates with good electrical conductivity and electrochemically active oxygen atoms were obtained. This study suggests that the large hole structure benefits mass transfer.[70] Thus, it is worth noting that the overall performance of these nanographenes is directly related to their nanostructures, providing an opportunity for boosting ORR activity by structural modulation enabled by defects, size, and doping.

3. Modulation on Intrinsic Defects of Nanographenes for ORR

In the synthesis of graphene, the production of a certain level of disorder and intrinsic defects is inevitable (Figure 2).[71] These defects typically arise from missing carbon atoms or the rearrangement of sp^2-hybridized carbon atoms, manifesting as vacancy defects (single or multiple vacancies)

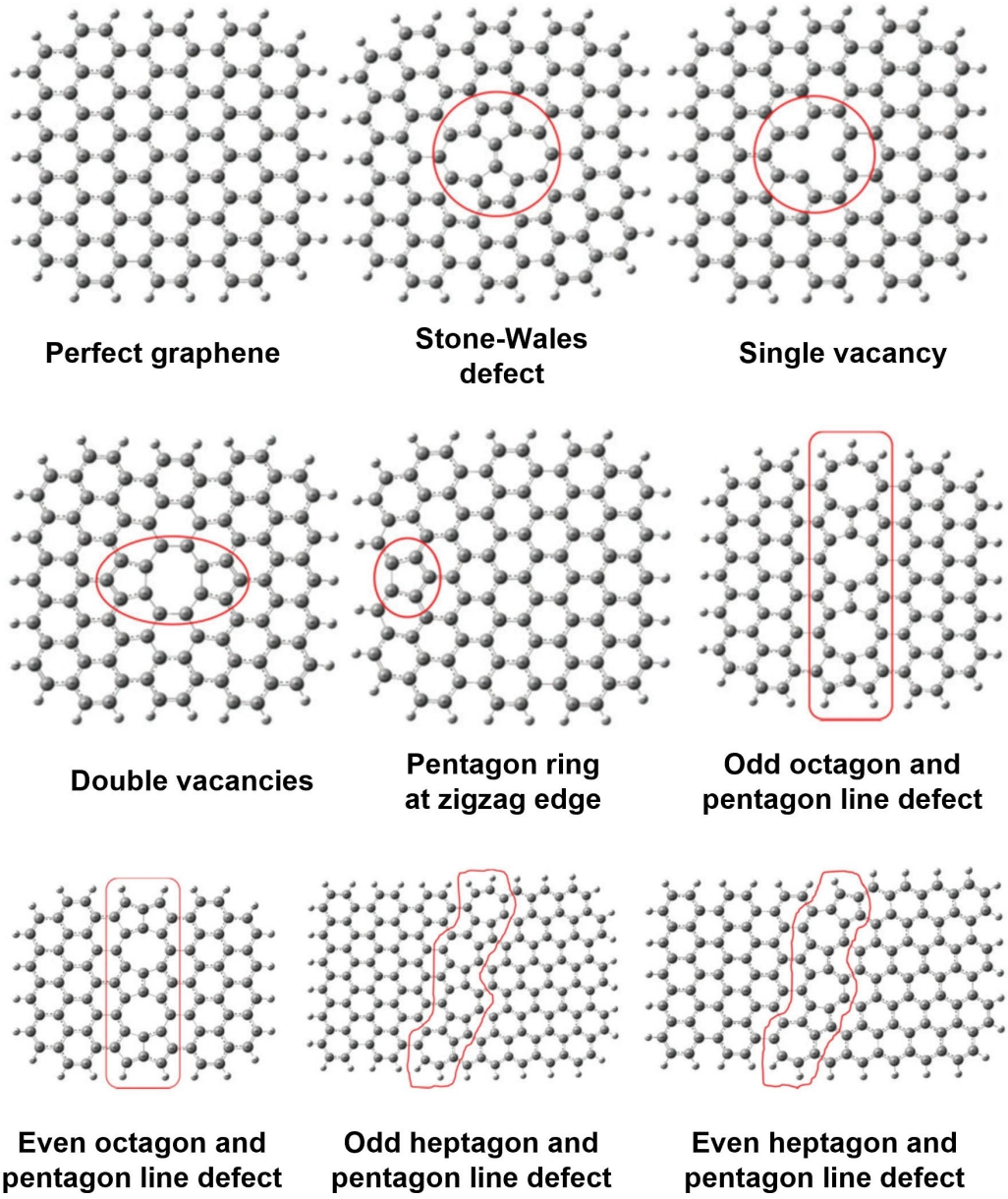

Figure 2. Structure model of perfect and defective graphene. (Reproduced with permission from,[71] copyright 2021, The Royal Society of Chemistry).

or topological defects (e.g., Stone-Wales Defects), all categorized as point defects. Besides, line defects like grain boundaries can also be found on the surface of defect-rich graphene.[71] These point and line defects influence the local charge distribution at carbon sites, consequently affecting the adsorption behavior of oxygen intermediates. The defect position can result in varying charge distributions, thereby influencing the activity of active sites.

O_2 adsorption on carbon sites is an endothermic process, and the smooth adsorption of oxygen is crucial for the progression of the ORR reaction.[72] At the edge site of the pristine carbon catalyst, from theoretical calculations, the total energy monotonically increased as the O_2 molecule approached the carbon active site (C_{ad}). This increase continues until the C–O bond length reaches 1.57 Å, corresponding to an energy barrier of 0.25 eV, suggesting unfavorable O_2 adsorption (Figure 3a).[73] In fact, most defects exhibit enhanced oxygen adsorption capacity.[74] Specifically, point defects with pentagon rings at zigzag edges and line defects like pentagon-pentagon-octagon and pentagon-heptagon chains at the edges demonstrate superior catalytic activity for ORR.[75] It is suggested that the higher spin and charge density at the zigzag edge facilitates the adsorption of OOH/O_2 molecules, enhancing catalytic activity for ORR (Figure 3b).[75] However, through computational screening of numerous sites, Choi et al. discovered that defects don't directly alter the electronic structures of Cad, but rather enhance its structural flexibility.[73] In the first edge-closest defective carbon model (DV1), no O_2 molecule is adsorbed on the C_{ad}, whereas the second edge-closest defective model (DV2) demonstrates successful adsorption, suggesting that geometric structure is a key factor in O_2 adsorption (Figure 3c). The chemical adsorption of O_2 often involves the sp^2/sp^3 transformation of C sites, consuming significant energy and resulting in a high energy barrier for chemical reactions. In defective models with O_2 adsorption, the bond lengths between C_{ad} and the adjacent carbon atoms increased by 0.07–0.08 Å (Figure 3d), similar to the pristine carbon model, indicative of sp^3-hybridization. In contrast, the bond lengths between the second carbon atoms away from the C_{ad} in defective models alter by 0.04–0.06 Å, compared to a change of approximately 0.01–0.02 Å in the pristine model. These findings indicate that the weaker C–C bonds surrounding vacancies contribute to structural flexibility, effectively relieving strain and thus reducing the energetic cost of O_2 adsorption.

A significant milestone was reached with the experimental demonstration of defect-induced electrocatalytic ORR activities in a catalyst composed of graphene quantum dots supported by graphene nanoribbons.[58] Numerous surface and edge defects at the surface and interface were confirmed to be the main active sites, although trace metals were also present. For the first time, Dai et al. developed a dopant-free and defect-rich graphene using Ar-plasma etching, which showed an onset potential of around 0.87 V.[44] Planar vacancy defects and edge defects with higher charge densities endowed advanced ORR performance to graphene. An edge-rich carbon nanotubes and graphite can

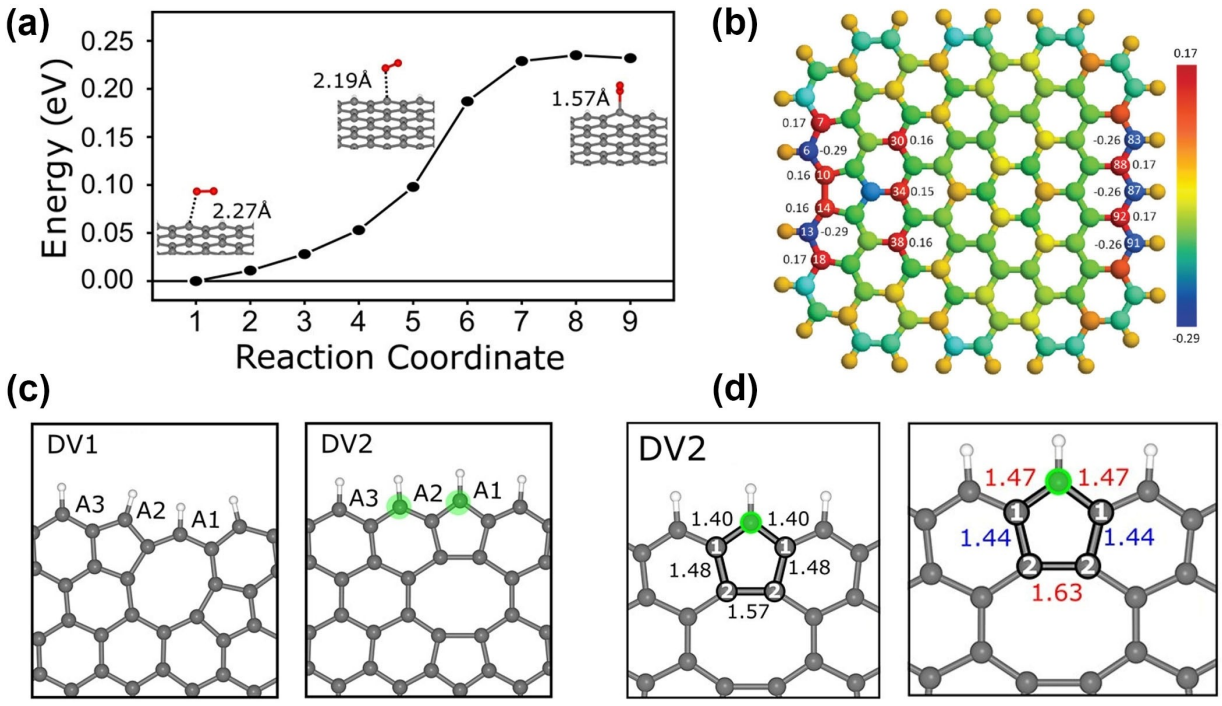

Figure 3. (a) Energy profile during the approach of O_2 to a defect-free nanoribbon (Reproduced with permission from,[73] copyright 2022, American Chemical Society). (b) Charge density distribution on graphene cluster with a pentagon ring at the zigzag edge (Reproduced with permission from,[75] copyright 2015, The Royal Society of Chemistry). (c) The defective carbon model with divacancy located at different positions. The green circles represent the possible adsorption sites and (d) Bond lengths before and after O_2 adsorption on the DV2 model (Reproduced with permission from,[73] copyright 2022, American Chemical Society).

also be obtained by a similar strategy and show enhanced ORR activity. In addition to partial carbon atom etching, removing heteroatoms such as doped N atoms also creates defect-rich sites on graphene.[76–77] By employing a simple annealing process, N atoms can be removed from N-doped graphene, resulting in a structure rich in holes and defects (including pentagons, heptagons, and octagons).[76] The defect-rich graphene demonstrated high activity not only in alkaline ORR but also in HER and OER. Based on the observation from TEM, four computational models were established by theoretical calculations, including edge pentagon, 585, 7557, and 5775 defects (Figure 4a). Unexpectedly, the 5775 model exhibited no catalytic activity for ORR, OER, or HER. Among other models, only five specific defect atomic sites (5–1, 585–1, 585–3, 7557–1, and 7557–4) demonstrated competitive catalytic activity (Figure 4b). It was found that the edge sites in edge pentagon, 585, and 7557 models exhibit a lower activation barrier toward ORR, further confirming the dominance of edge defect sites.

In acidic ORR, the detailed catalytic mechanism and identification of the active sites (especially for the co-existence of N-doped sites and carbon defect sites) have been controversial for a long time. Recent studies have confirmed that topological carbon defects contribute to higher ORR activity, whereas N-doped sites become inactive due to the protonation of pyridinic nitrogen (Pr–N) sites.[78–79] To pinpoint the actual active sites for acidic ORR, Yao et al. precisely prepared a topological defect-rich carbon catalyst by removing N-dopants.[77] Notably, the removal of Pr–N facilitates the controlled formation of edged pentagon defects (Figure 4c). Theoretical calculations confirm that the formation energy of two pentagons is lower than that of divacancy from removing of the zigzag Pr–N and armchair Pr–N, as well as HAADF-STEM images show only pentagon sites in defective graphene derived from N-

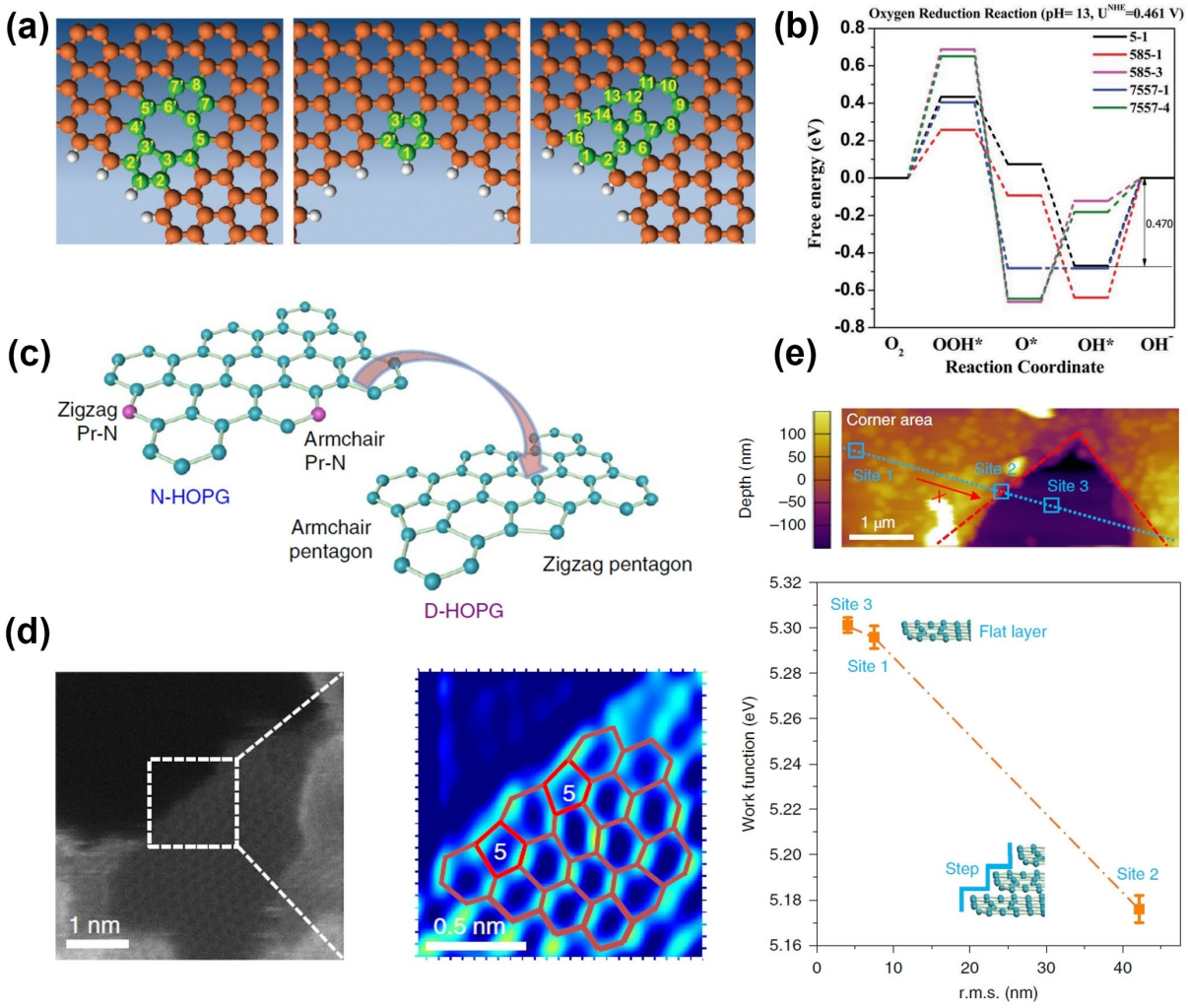

Figure 4. (a) Structure model of pentagon defect, 5–8–5 defect, and 7–55–7 defect and (b) Schematic energy profiles for the ORR pathway on a series of defect models. (Reproduced with permission from,[76] copyright 2016, WILEY-VCH Verlag GmbH & Co. KGaA, Weinheim). (c) Illustration of the edge defect reconstruction that originated from nitrogen removal, (d) The HAADF-STEM image of the derived defective graphene and the corresponding color gradient image, and (e) Local work functions collected from three different regions on defective highly oriented pyrolytic graphite. (Reproduced with permission from,[77] copyright 2019, Springer Nature).

doped graphene (Figure 4d). Work function analyses revealed that edged pentagon defects lower the local work function, facilitating electron transfer from active sites to adsorbed O_2 molecules and promoting the generation of OOH species (Figure 4e). While significant progress has been made in the study of graphene with topological defects, most research has concentrated on the edge sites. Further fundamental research is needed on planar defect structures and their associated electrocatalytic properties. Additionally, the stability of defect-rich catalysts must be established before their practical applications can be realized.

4. Modulation on Size of Nanographenes for ORR

The size effect is a well-established strategy for fine-tuning catalytic activity in various industrial reactions.[80] This approach has been extensively investigated in electrocatalytic reactions, such as optimizing ORR activity on Pt nanoparticles between 3 to 5 nm[81] and the size-dependent selectivity and activity observed on Cu nanoparticles for electrochemical CO_2 reduction.[82] Given the two-dimensional structure of graphene, with its anisotropic properties in lateral and basal planes, the size effect is expected to influence ORR electrocatalysis differently in these dimensions.

Much of the current research focuses on controlling the size of nanographenes primarily in the lateral direction. This focus stems from observations that ORR activity is higher at the edge sites of highly oriented pyrolytic graphite (HOPG) than at its basal sites, as measured in micro-electrochemical systems.[83] Consequently, several synthetic methods have been developed to achieve nanographenes with controllable lateral sizes that expose more edge sites. For instance, Deng et al. employed a straightforward ball milling method to modulate the size of graphene derived from graphite powder (GP), resulting in sizes ranging from 20 to 100 nm by adjusting the milling duration.[33] It was found that graphene size only dramatically reduces within the first 3 hours as shown in Figure 5a. Electrochemical measurements showed ORR current increases with the decrease of graphene size at several fixed voltages, including −0.2, −0.15, and −0.1 V (vs. Hg/HgO), as shown in Figure 5b. The size effect becomes more significant below 100 nm (Figure 5c). The higher ORR activity of nanographenes with smaller sizes is attributed to the more zigzag edges with oxygen-containing groups. Although graphite-derived nanographenes via ball milling showed a clear trend of size-dependent activity, it is inevitable that the size distribution of obtained nanogra-

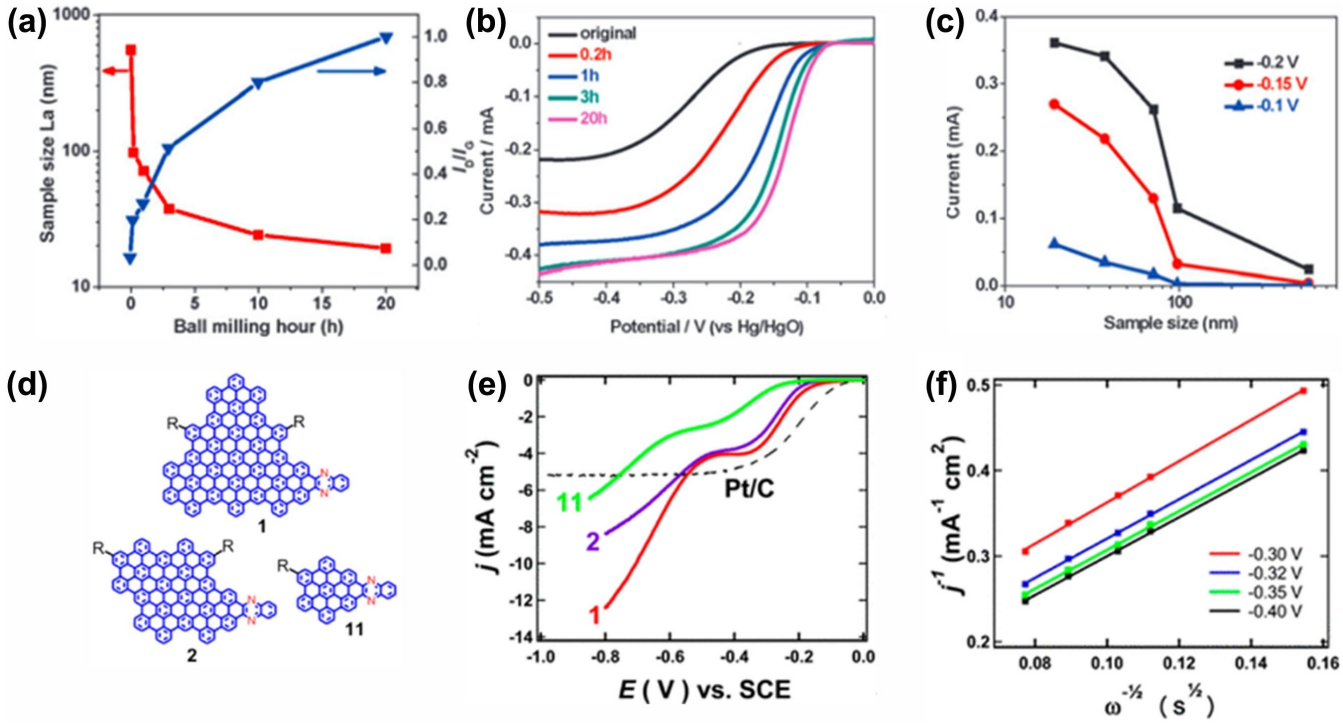

Figure 5. (a) The I_D/I_G from Raman and the estimated lateral size L_a of GP-BM as a function of ball milling duration, (b) ORR voltammogram of GP and GP-BM catalysts resulting from ball milling for different durations and (c) The size effect of graphene on the electroactivation of oxygen by referring to the oxygen reduction current at the potential of −0.1, −0.15 and −0.2 V, respectively. (Reproduced with permission from,[33] copyright 2011, The Royal Society of Chemistry) . (d) Structures of N-doped GQDs with different sizes and (e) LSV curves (10 mV s^{-1}) for 1–3 and Pt/C on a RDE (1600 rpm) in an O_2-saturated 0.1 M KOH solution. Also shown is the LSV curve for 11, a much smaller N-substituted heterocycle with structure shown in the inset. (Reproduced with permission from,[34] copyright 2012, American Chemical Society). (f) Koutecky–Levich plots for 1 obtained from the LSV curves. A global fitting of the plots reveals that the number of electrons transferred per O_2 molecule is 3.9. (Reproduced with permission from,[34] copyright 2012, American Chemical Society).

phenes might not be as narrow as enough. GQDs, categorized as zero-dimensional carbon materials, offer unique characteristics owing to their nanometer-sized lateral dimensions and thinness, typically consisting of single or few layers with thicknesses below 10 nanometers. These dimensions endow GQDs with intriguing edge effects and properties arising from quantum confinement.[84] A study by Li et al. demonstrated that nitrogen-doped GQDs exhibited electrocatalytic activity comparable to that of a commercially available Pt/C catalyst for ORR in an alkaline medium.[85] The feature of atomic-sized structures and high ORR catalytic activity of doped GQDs allows them to be a relatively ideal material platform for investigating the size effect on electrocatalytic activity. Another work from Li et al. reported a solution chemistry approach to synthesize nitrogen-doped GQDs by using small substituted benzene derivatives as the starting material, as shown in Figure 5d.[34] With such a bottom-up synthesis, they could precisely control the number of nitrogen atoms and define their bonding configurations. The size of prepared GQDs was further characterized by mass spectroscopy and UV-vis absorption spectra. The linear sweep voltammetry (LSV) shows a size-dependent electrocatalytic activity phenomenon in N-GQDs. GQDs with greater molecular weights exhibit improved catalytic activity (Figure 5e). This is because larger QDs are more easily oxidized with higher occupied molecular orbital (HOMO) levels. Further analyses on the slope of the Koutecky–Levich plots in Figure 5f, the number of electrons transferred per oxygen molecule in the ORR is calculated to be about 3.9, suggesting a four-electron ORR process.

The size effect discussed above concerns the lateral dimension. However, size in the thickness direction is also likely to play a role, as thinner graphene sheets have more exposed edge sites. This idea has been verified by Benson et al., who reported considerably higher electron transfer numbers on graphene nanosheets compared to the thicker graphene nanoplatelets.[47] Besides, electronically conductive carbon layers are usually used as the substrate to support other active electrocatalysts for ORR. Hof et al. reported the lateral dimension of the carbon layer effectively affects the size distribution of deposited iron oxide nanoparticles,[86] which is controlled by the availability of electrons on individual graphene sheets, where larger carbon lattices lead to the formation of larger particles. The redox process for iron oxide deposition is primarily governed by the surface reaction rate rather than diffusion, facilitated by the high electron mobility and low electron transfer energy on the carbon lattice. The resultant composite catalyst with the smaller size of carbon lattices exhibited an ORR onset potential (+0.79 V vs. RHE), 40 mV more positive than medium-sized nanoparticles and 60 mV more positive than large-sized nanoparticles. The electron transfer number of smaller-sized nanoparticles was 3.6 at the potential of 0.45 V, revealing that it proceeds mainly by a four-electron pathway. In comparison, the medium-sized and larger-sized nanoparticles exhibit lower electron transfer numbers of 3.37 and 2.96, respectively, suggesting two- and four-electron mixed transfer processes.

While experimental efforts have focused on understanding the size effect of nanographenes on ORR, challenges remain in precisely controlling nanographenes size and obtaining accurate experimental measurements, complicating the optimization process for ORR. Theoretical approaches, such as density functional theory (DFT) calculations, provide a valuable alternative by offering atomic-scale insights into electronic structures and their relationship with catalytic activity. These methods help elucidate the ORR mechanism and the size effect on structure-activity relationships. Zhang et al. optimized structures of N-doped GQDs based on DFT calculation and found the three most stable atomic structures with different sizes, i.e., $C_{23}H_{12}N$, $C_{53}H_{18}N$, and $C_{95}H_{24}N$ as depicted in Figure 6a.[35] The free energy diagrams for ORR on these GQDs, as shown in Figure 6b–d, suggested the rate-determining step locates the step of the formation of the second H_2O molecule at electrode potential U = 1.23 V. The results indicated that the smallest N-doped GQDs had the smallest overpotential and the highest ORR catalytic activity, due to its weakest adsorption of ORR intermediates and easiest C–OH bond break for the formation of second H_2O molecule. Against the conventional wisdom that O_2 adsorption must precede the electron transfer (ET) step, it was suggested by Choi et al. that the first electron transfer into O_2 molecules takes place at the outer Helmholtz plane (ET-OHP).[45] This new concept challenges the conventional belief that an active site must possess as good an O_2 binding character as that which occurs on metallic catalysts. Based on the ET-OHP mechanism, the location of the electrode potential dominantly characterizes the ORR activity as shown in Figure 6e–2f. Accordingly, they demonstrate that the electrode potential can be elevated by reducing the graphene size and/or including metal impurities, thereby enhancing the ORR activity.

While most studies on the size effect of nanographenes for ORR focus on the four-electron process, there is also evidence that this effect can facilitate the ORR through a two-electron pathway. This pathway, used for the electrosynthesis of H_2O_2, has gained significant interest as a potential replacement for the traditional energy-intensive, multi-step anthraquinone process.[87] Matsuyama et al. investigated the ORR selectivity of N-doped graphene nanoclusters (N-GNCs) using first-principles calculations within the DFT.[88] The results showed that high selectivity toward the $4e^-$ pathway is attained for GNCs with N atoms located at the inner doping sites of the cluster rather than at the edge sites. The results also reveal that the water molecule generated by the ORR enhances the selectivity toward the 4e pathway because the reaction intermediates are significantly stabilized by water. The same group used DFT-based first-principles calculations to examine how the size of N-GNCs affects ORR activity and selectivity.[46] Regarding the cluster size, it was discovered that the maximum electrode potential (U_{Max}) of the ORR shows a volcanic trend. According to their predictions, $C_{215}H_{36}N$, an N-GNC with a radius of 13.6 Å, is the best option for ORRs and performs better than platinum in terms of U_{Max}. As can be seen from Figures 6g–h, all models have the selectivity for the $4e^-$

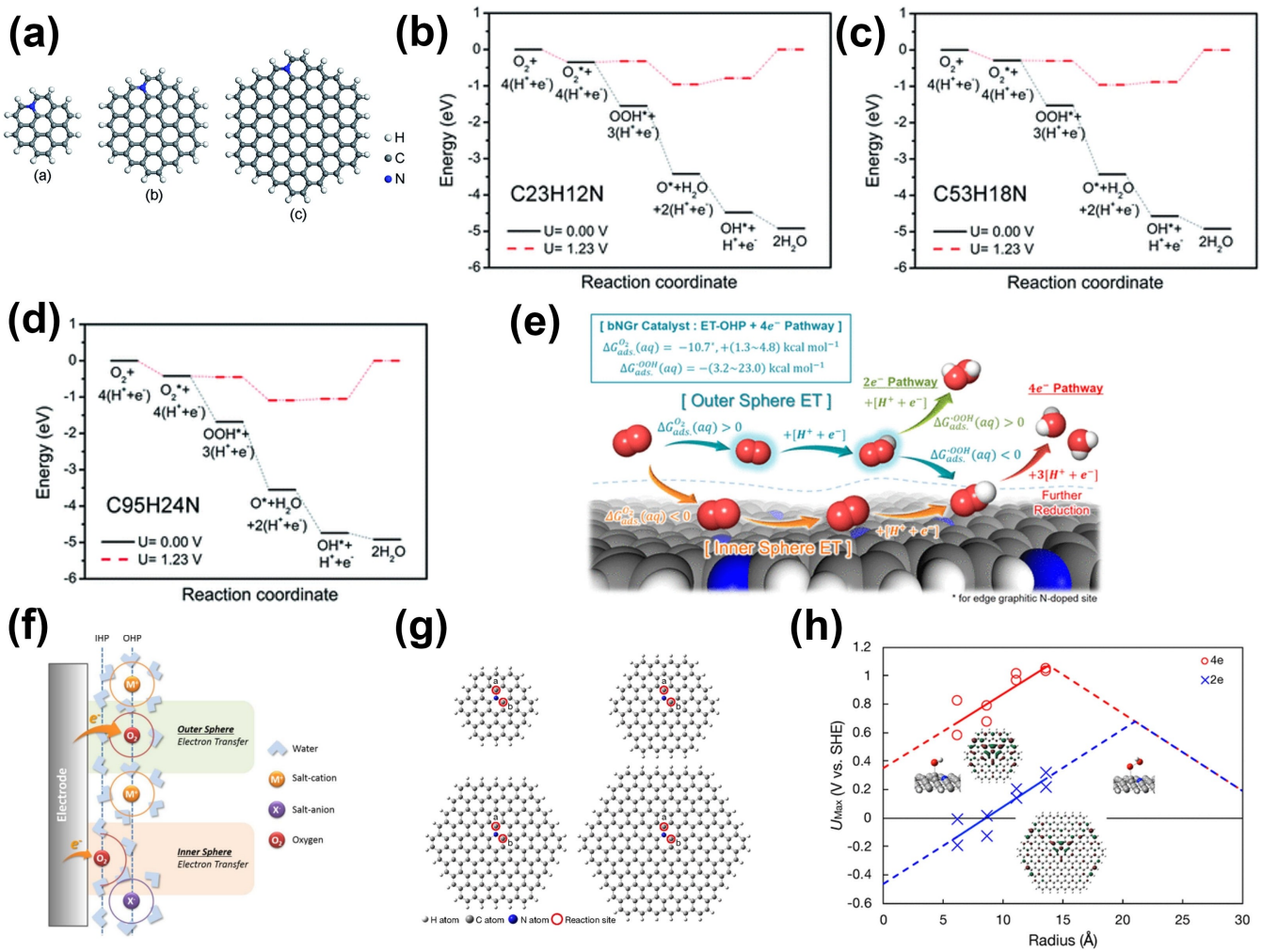

Figure 6. (a) Optimized structures of N-doped graphene quantum dots $C_{23}H_{12}N$, $C_{53}H_{18}N$, and $C_{95}H_{24}N$ and (b–d) Schematic Gibbs free energy diagrams of ORR on $C_{23}H_{12}N$, $C_{53}H_{18}N$, and $C_{95}H_{24}N$ models. (Reproduced with permission from,[35] copyright 2018, The Royal Society of Chemistry). (e) ORR pathway starting from the solvated O_2 molecules: ET-OHP and ET-IHP Processes and (f) Schematic diagram of the difference between first electron transfer kinetics for ORR. (Reproduced with permission from,[45] copyright 2014, American Chemical Society). (g) Models of the following N-GNCs: $C_{53}H_{18}N$, $C_{95}H_{24}N$, $C_{149}H_{30}N$, and $C_{215}H_{36}N$ and (h) U_{Max} values of the N-GNCs with various sizes. The circles and the crosses show the U_{Max} values calculated for the $4e^-$ and the $2e^-$ pathways, respectively. The solid and dashed lines show values of U_{Max} calculated from the fitted and extrapolated values for ΔG_{diff}, respectively. (Reproduced with permission from,[46] copyright 2022, American Chemical Society).

pathway. Meanwhile, there is no selectivity for the $4e^-$ pathway, and U_{Max} values are lower than those of N-GNCs when the particle size is larger than around 20 Å. Because of the destabilization of reaction intermediates, which causes the reaction step that determines U_{Max} to change, the U_{Max} plot takes on the shape of a volcano. The study concludes that the development of edge states at the zigzag edges of N-GNCs influences the local density of states at the reaction site, affecting the stability of the reaction intermediates.

5. Modulation on Electronic Structure by Dopants into Nanographenes for ORR

Introducing heteroatoms like nitrogen, sulfur, phosphorus, or boron into graphene significantly enhances its ORR performance. Doping with elements of varying electronegativities allows for the control of charge density on neighboring carbon atoms, influencing oxygen adsorption and charge transfer dynamics. This section explores the effects of dopants on graphene's oxygen electrocatalysis performance and their influence on the electronic structure.

5.1. Single Heteroatom Doping

Since Dai et al.'s 2009 report on the high ORR activity of vertically aligned nitrogen-containing carbon nanotubes, extensive research has focused on elucidating the reaction mechanism and enhancing ORR activity in nitrogen-doped carbon materials.[89] In 2010, Dai et al. first introduced nitrogen-doped graphene catalysts for ORR, demonstrating ORR performance comparable to nitrogen-containing car-

bon nanotubes (Figure 7a).[90] The higher electronegativity of nitrogen compared to carbon enables nitrogen atoms to attract more electrons and modulate the electronic structure of carbon active sites. Due to their proximity on the periodic table and similar chemical properties, nitrogen atoms can substitute carbon atoms in various positions. Depending on the doping position, nitrogen doping is categorized into three types identifiable by XPS N 1s spectra: pyridinic N (398.5 eV), pyrrolic N (400.1 eV), and graphitic N (401.1 eV).[91–92] The presence of mixed nitrogen species in N-doped carbon materials poses challenges in identifying the active sites.

Ex-situ XPS measurements on N-doped highly oriented pyrolytic graphite (N-HOPG) revealed a decrease in pyridinic-N and an increase in pyrrolic/pyridonic-N post-ORR, while their total remained unchanged. This suggests that carbon sites near pyridinic-N interact with OH species during ORR (Figure 7b).[91] Nakamura et al. proposed that the active sites for ORR in N-doped carbon materials are the carbon atoms next to pyridinic N. ORR catalytic measurements showed that ORR performance in N-HOPG and N-doped graphene improves with higher pyridinic-N levels, regardless of other N species' concentrations (Figure 7c–e). DFT calculations, scanning tunneling microscopy/spectroscopy (STM-STS), and CO_2 temperature programmed desorption (TPD) measurements confirmed that carbon sites adjacent to pyridinic-N are Lewis basic sites, preferred for oxygen molecule adsorption.[91, 93] Utilizing the electrophilic feature of pyridinic N and the selective capture of free radicals by adjacent C atoms, Sun et al. used acetyl chloride and acetyl radical to prepare acetyl group modified N atom (N_Ac) and C atom (C_Ac), respectively.[94] N_Ac exhibited similar ORR performance to the original N-doped graphene, while C_Ac was ORR inert, further confirming the activity of C atoms adjacent to pyridinic-N. Conversely, Liu et al. concluded that electron-donating graphite-N facilitates ORR and electron-withdrawing pyridinic-N is key for OER, based on Mott-Schottky and ultraviolet photoelectron spectroscopy (UPS) analyses.[95] To conclusively resolve debates on active sites, synthesis methods must be developed for N-doped carbon materials with single-species N doping.

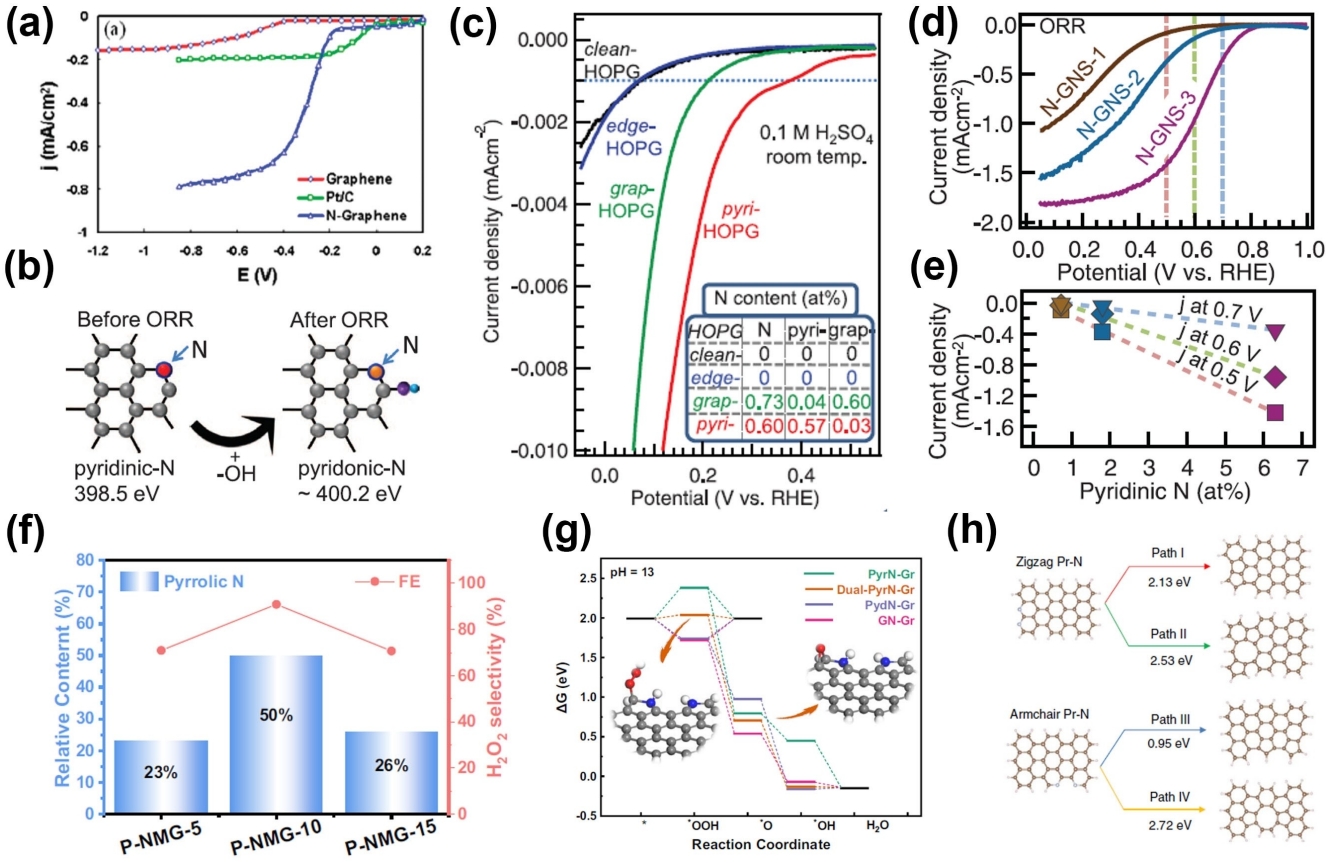

Figure 7. (a) LSV curves for ORR at graphene, Pt/C, and N-doped graphene electrode. (Reproduced with permission from,[90] copyright 2010, American Chemical Society). (b) Schematic representations of pyridinic nitrogen formation through OH attachment to the carbon atom adjacent to pyridinic N, (c) ORR LSV curves for HOPG doped with various nitrogen species, (d) ORR LSV curves for N-doped graphene with varying concentrations of pyridinic-N dopants and (e) the corresponding relationship between current densities and concentrations of pyridinic-N. (Reproduced with permission from,[91] copyright 2016, American Association for the Advancement of Science). (f) Correlation between pyrrolic N levels and H_2O_2 selectivity and (g) Free energy profile for $2e^-$ and $4e^-$-ORR pathways on various N-doped graphene types. (Reproduced with permission from,[40] copyright 2023, Springer Nature). (h) Four pathways to carbon defects from zigzag and armchair pyridinic-N structures. (Reproduced with permission from,[77] copyright 2019, Springer Nature).

Unlike pyridinic-N and graphite-N, which prefer the 4e⁻-ORR pathway, pyrrolic-N may demonstrate a high selectivity for the 2e⁻-ORR pathway due to its low adsorption affinity for OOH intermediates. To improve H_2O_2 selectivity in ORR, Liang et al. developed a graphene/mesoporous carbon composite (P-NMG–X) featuring multiple pyrrolic N sites created by pyrolyzing a blend of F127, resol, and melamine.[40] By adjusting the melamine to resol ratio, a pyrrolic-N-rich catalyst, P-NMG-10, was produced, achieving a pyrrolic-N content of 50 %, equivalent to an atomic ratio of 4.7 at. %. Electrocatalytic ORR tests revealed a positive correlation between H_2O_2 selectivity and pyrrolic-N content (Figure 7f). Theoretical calculations showed that dual-pyrrolic-N sites exhibit nearly zero overpotential for OOH formation (Figure 7g), the only intermediate for the 2e⁻-ORR pathway. Meanwhile, single pyrrolic-N sites and pyridinic-N/graphite-N sites demonstrate respectively too weak and too strong adsorption to OOH. These findings suggest that the adsorption capacity of active sites for OOH intermediates influences the selectivity between the 4e⁻ and 2e⁻-ORR pathways.

N-doped carbon materials commonly feature topological defects such as vacancies, with N dopants favoring these defect sites. DFT calculations show that N dopants favor locations near defects energetically, particularly at sites with significant bond shortening.[96] It is also found that the presence of carbon defects shifts the N doping process from endothermic to exothermic. Pyridinic-N shows greater stability at monovacancy defects, whereas pyrrolic-N tends to form at Stone-Wales and divacancies defects. However, experimentally, N-doped graphene with the fewest carbon lattice defects demonstrated the highest H_2O_2 selectivity. Post-H_2O_2 treatment, N-doped graphene showed increased in-plane carbon vacancy density but lower H_2O_2 selectivity in ORR.[41] The ease of pyridinic-N formation at defect edges likely led to an abundance of pyridinic-N in H_2O_2-treated N-doped graphene, resulting in poor H_2O_2 selectivity. A defect-rich graphene nanomesh, created by thermal exfoliation of metal-organic frameworks, demonstrated that 4e⁻-ORR performance positively correlates with defect density, suggesting vacancy defects in N-doped carbon materials enhance 4e⁻-ORR.[97] Additionally, removing certain N species can lead to specific carbon topological defects (Figure 7h).[77] These findings indicate a significant cooperative effect between carbon defects and N dopants, crucial for tuning ORR performance.

Beyond N dopant, doping graphene with other heteroatoms, like B, P, S, and O can also regulate the electronic structure and ORR performances.[98–99] DFT calculations reveal that B-doped graphene shows nearly zero overpotential for H_2O_2 formation, whereas P- and S-doped graphene present higher energy barriers (Figure 8a–e).[100] Despite favoring the 4e⁻-ORR pathway, B-doped carbon materials achieve an H_2O_2 selectivity of 85 % across a wide potential range. Molecular dynamics simulations with explicit solution models calculated the OOH^- formation barrier as 0.53 eV and the O formation barrier as 0.70 eV, suggesting the 2e⁻-ORR pathway is more favorable in B-doped graphene (Figure 8f). Moreover, the 2e⁻-ORR performance of B-doped rGO was endowed with the doped B element, unaffected by the oxygen functional group or defects.[101] O dopants also enhance H_2O_2 selectivity in ORR, with DFT calculations showing that C=O and defective C–O–C groups optimally adsorb OOH, resulting in the lowest overpotential for H_2O_2 production (Figure 8g).[99, 102] The graphene oxide subjected to mild thermal reduction, featuring ring ether and epoxy groups at basal planes and edges, demonstrated outstanding H_2O_2 selectivity.[102] The P-doped graphene exhibits the potential for 4e⁻-ORR.[38, 98] The P dopants can form three or four P–C bonds (PC3G or PC4G), which are easily oxidized into the OPC3G and OPC4G with P–O bond. Among all structures, OPC3G and OPC4G exhibit optimal catalytic ORR activity, whereas PC3G shows the least, attributed to its poor stability and conductivity.[98]

5.2. Multiple Heteroatom Doping

As discussed above, N dopants demonstrate significant promise for 4e⁻-ORR. Doping with additional elements can further adjust the work function and energy gap, enhancing charge transfer and increasing active sites.[42, 103–104] Following the development of N-doped graphene for ORR, Dai et al. advanced B, N co-doped graphene, confirming its optimal ORR activity and stability with moderate doping levels.[104] The significant electronegativity difference between B and N facilitates B–N bond formation in graphene.[105] More recently, pyridinic-N–B pairs have been identified for the 4e⁻-ORR, characterized by low energy barriers and high stability.[103] B dopants can bond with pyridinic-N (B@PyN), pyrrolic-N (B@Pyrr), and graphite-N (B@GyN), forming B–N bonds (Figure 9a). It was found that the B atoms in B@GyN were identified as active sites, whereas C atoms adjacent to B in B@PyN facilitate ORR. Charge analysis of DFT calculation showed that C atoms near B atoms hold extra electrons, likely making them active sites. Additionally, two B–N (2B@PyN) structures carry more electrons than B@PyN. Consequently, the 2B@PyN and B@PyN showed optimal adsorption capacity towards *OH and the lowest overpotential. In combination with S dopants, graphite-N showed superior ORR activity, while pyrrolic-N and pyridinic-N demonstrated bifunctional ORR and OER activities.[106] Free energy calculations indicate that C3 sites near graphite-N with thiophenic-S have the lowest ORR overpotential (Figure 9b). It is observed that the graphite-N, S co-doped graphene possessed a high value of P partial density of state overlap at the Fermi level, suggesting enhanced electrical conductivity and faster charge transfer.

The N, O co-doped graphene also displayed bifunctional capabilities for both ORR and OER.[107] Unlike S dopants, the pyridinic-N and O dopant configuration is more stable. In the ORR pathway, introducing O significantly lowers the energy barrier for OOH formation, accelerating ORR kinetics (Figure 9c). The rate-determining step shifts from OH to *O formation in the OER pathway, indicating that O dopants in N-doped graphene enhance OH^- adsorption (Figure 9d). Adding P atoms to N-doped graphene also induces ORR and OER activity. Interestingly, the charge

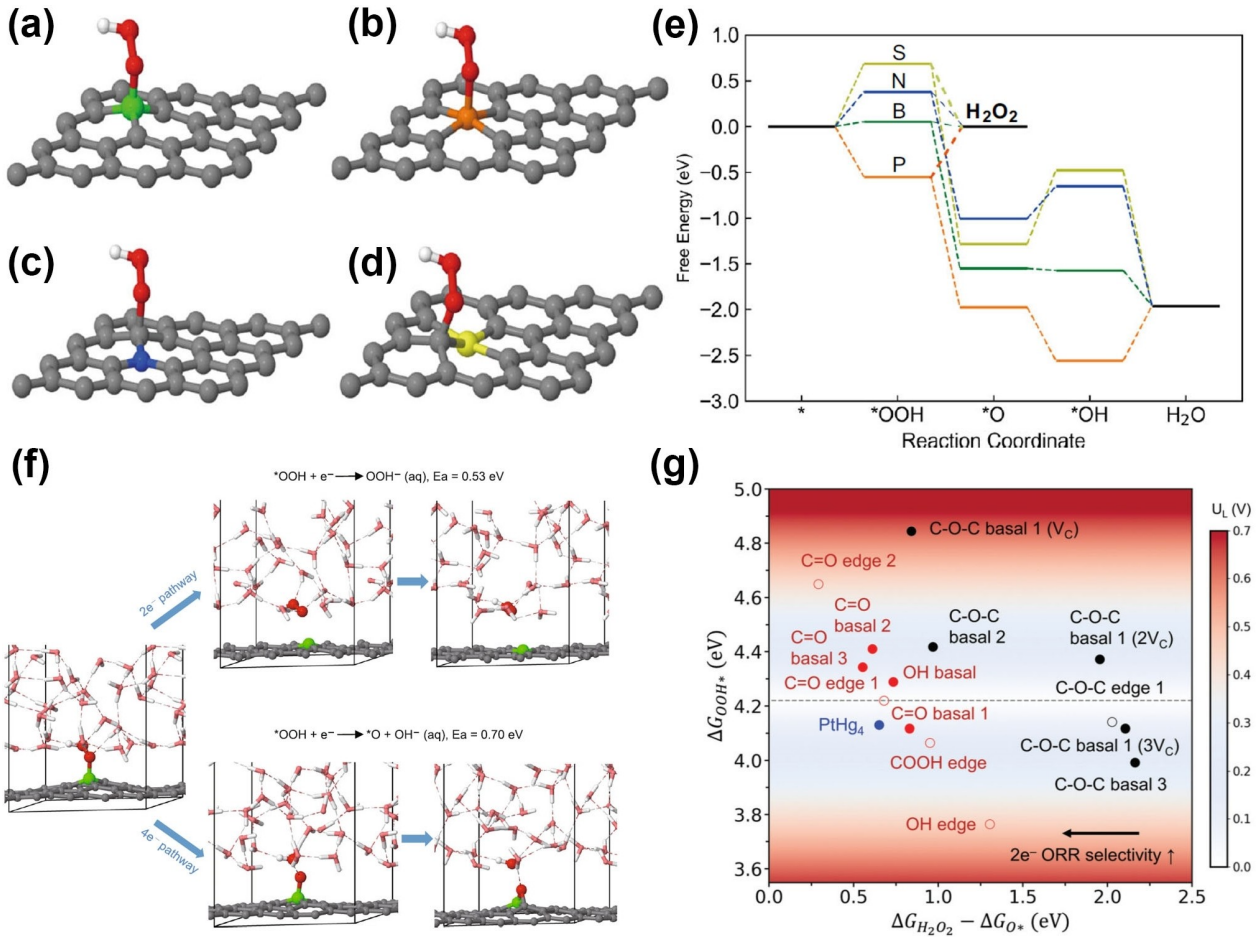

Figure 8. Preferred OOH adsorption configuration for (a) B-, (b) P-, (c) N-, and (d) S-doped graphene, respectively. (Reproduced with permission from,[100] copyright 2021, Springer Nature). (e) Free energy profile for ORR pathway and (f) The snapshots from molecular dynamics simulations for $2e^-$ and $4e^-$-ORR. (Reproduced with permission from,[100] copyright 2021, Springer Nature). (g) Scaling relationship for ΔG~OOH~ and $\Delta G_{H2O2-\Delta GO}$ across various oxygen functional groups. (Reproduced with permission from,[99] copyright 2022, The Royal Society of Chemistry).

and spin densities of active carbon atoms vary with the combination of P atoms and various N configurations.[108] In the case of graphite-N + pyridinic-N + P, over 35 % of carbon atoms (C_3) exhibit a charge density above 0.15, and 56.78 % have positive spin density, resulting in the lowest ORR overpotential (Figure 9e). Conversely, in the pyridinic-N + pyrrolic-N + P configuration, carbon atoms (C_4) with 11 % high charge density and 35 % positive spin density exhibit the lowest OER overpotential (Figure 9e).

Dai et al. further advanced tri-doped graphene (N, P, F) as a multifunctional catalyst for ORR, OER, and HER, demonstrating the significant potential for water-splitting and Zn-air batteries.[110] For a N, P, and S tri-doped graphene, the synergistic effect endowed graphene with high activity for OER and ORR (Figure 9f).[109] N dopants, with their high electronegativity (3.04), induce a positive charge density on adjacent carbon atoms, enhancing oxygen adsorption. The lower electronegativity of P (2.19) improved the electron delocalization in carbon atoms. Consequently, the abundant active sites and charge delocalization contribute to exceptional oxygen electrocatalytic activity, with graphite-N and pyridinic-N confirmed as the active sites for ORR and OER, respectively (Figure 9g). As we can see, introducing two or three dopants into graphene further modulates charge and spin densities on active carbon atoms, providing multifunctional catalytic activity beyond ORR.

5.3. Edge Functionalization

As mentioned above, edge sites, such as defects or dopants, show higher activity compared to planar sites. Introducing defects or dopants at the edges of graphene sheets can create additional active sites for ORR. Additionally, attachment of functional groups or molecules (e.g., hydroxyl, carboxyl, or amine groups) to the edges of graphene sheets can increase the density of active sites and improve catalyst-reactant interaction. For instance, carbonyl (C=O) and hydroxyl (C–OH) can be introduced at both armchair and zigzag edges of graphene under ORR conditions.[39] It was found that the C=O group preferred to be located at zigzag edge sites, whereas armchair edges can accommodate both C=O and C–OH groups. DFT calculations indicate that basal and most edge vacancy sites were inert toward $2e^-$-

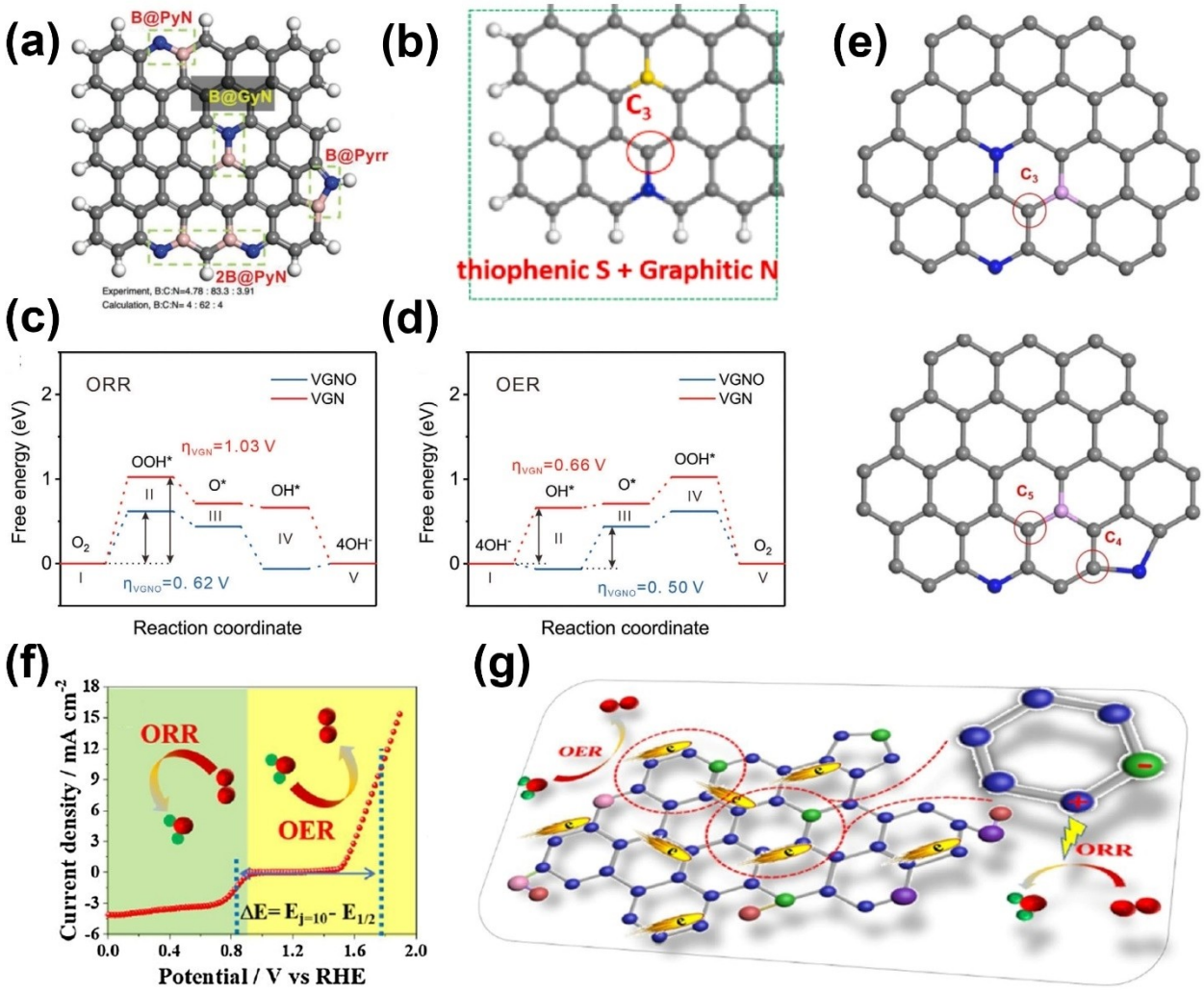

Figure 9. (a) Illustration showing ORR active sites in B, N co-doped graphene. (Reproduced with permission from,[103] copyright 2022, WILEY-VCH Verlag GmbH & Co. KGaA, Weinheim). (b) The constructed N, S co-doped graphene models. (Reproduced with permission from,[106] copyright 2022, Elsevier). Free energy profiles for (c) ORR and (d) OER for N, O co-doped graphene. (Reproduced with permission from,[107] copyright 2022, WILEY-VCH Verlag GmbH & Co. KGaA, Weinheim). (e) Structure models of various N, P co-doped graphene catalysts. (Reproduced with permission from,[108] copyright 2021, WILEY-VCH Verlag GmbH & Co. KGaA, Weinheim). (f) Overall LSV curve for N, P, S tri-doped graphene and (g) Structural configurations of doped heteroatoms in graphene for ORR and OER. (Reproduced with permission from,[109] copyright 2021, Elsevier).

ORR to H_2O_2 formation (Figure 10a–b). The zigzag sites with a high (3/4) coverage and armchair sites with a low (1/6) coverage of C=O groups exhibit the lowest overpotential for H_2O_2 formation (Figure 10c). Under thermal annealing, the edge carboxylic acid groups may decompose to generate ether functional groups at the edge, reducing the overpotential for $2e^-$-ORR to 10 mV.[102] Annealing rGO at 600 °C results in a significant decrease in carboxylic acid groups and a modest increase in ether C–O groups (Figure 10d). FTIR and O K-edge NEXAFS spectra confirmed that the ether functionalities were formed at the sheet edge of rGO (Figure 10e–f). Edge ring ether groups induce sp^2-hybridized carbon, enhancing interaction with adsorbed intermediates and increasing H_2O_2 formation activity.

While graphene edge functionalization offers a promising route to enhance ORR activity, critical issues need to be addressed, including the stability of the functionalized edges under operational conditions, control over the functionalization process for uniform and reproducible catalysts, and scalability of the production methods. Moreover, understanding the fundamental mechanisms of how edge functionalization affects ORR activity and durability is crucial for designing more efficient catalysts.

6. Synergistic Effect among Carbon Defects, Size Structure and Heteroatoms Doping for ORR

The individual effects of carbon defects, geometric size, and heteroatom doping in nanographenes on electrocatalytic ORR have been discussed earlier. This section focuses on

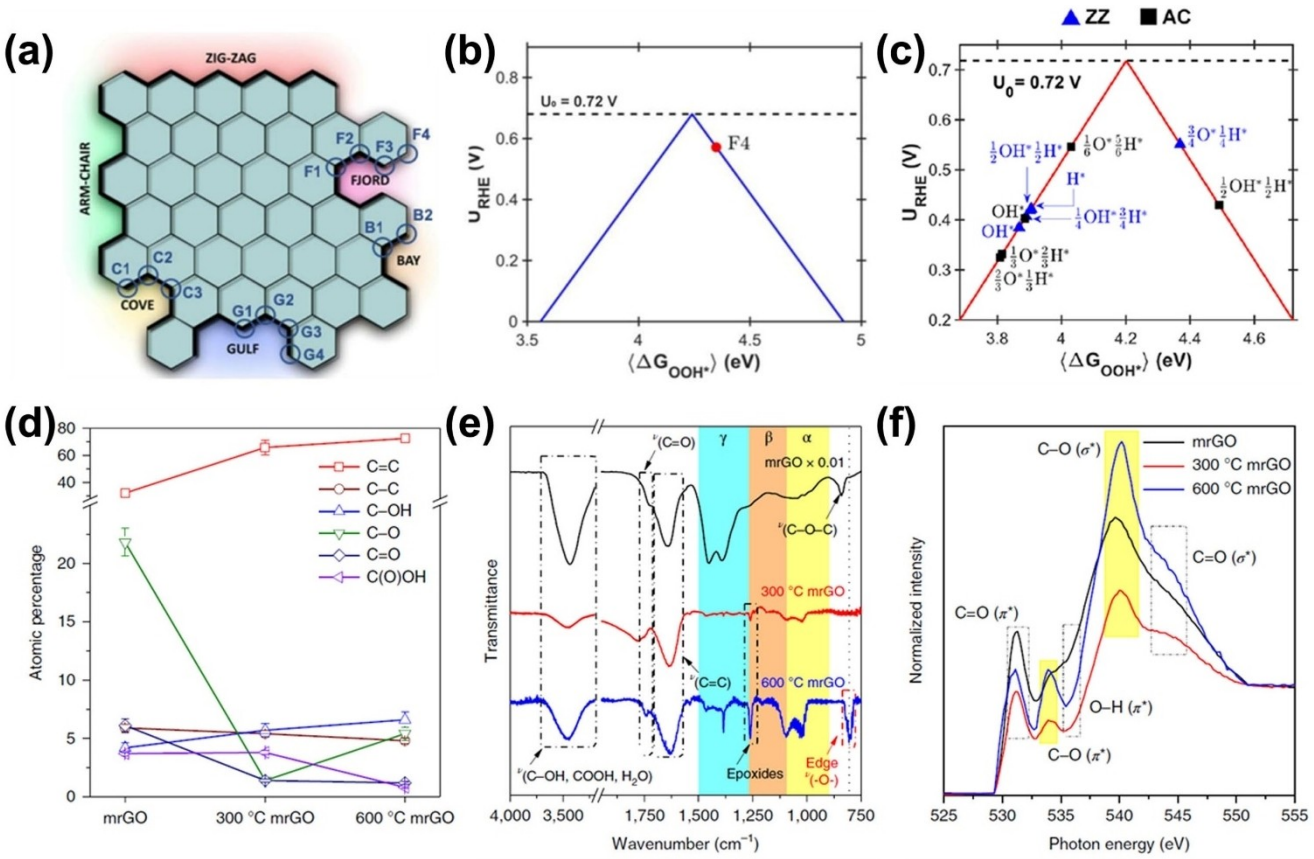

Figure 10. (a) Structural model of potential active sites in graphene with high vacancy defects, (b) Plot of activity against the free energy of OOH* adsorption across various defect sites, and (c) Theoretical activity volcano plot for 2e⁻-ORR. (Reproduced with permission from,[39] copyright 2020, American Chemical Society). (d) The atomic ratio in rGO and annealed rGO as measured by C 1s XPS, (e) FTIR and (f) O K-edge NEXAFS spectra for rGO and annealed rGO.

their combined impact on ORR performance. In practice, manipulating the size of nanographenes using various synthetic methods often leads to the concurrent formation of defects and heteroatom doping. For example, top-down techniques like ball milling, which enhance edge site exposure, typically create topological defects (non-hexagonal carbon structures) and introduce oxygen atoms or oxygen-containing groups along the nanographenes edges. Similarly, bottom-up approaches using large polycyclic heteroaromatic compounds can produce structures with inherent defects and dopants. As a result, carbon defects, size structure, and heteroatom doping are interconnected features when optimizing nanographenes for ORR applications. Significant research has focused on understanding the synergistic effects among these three strategies to elucidate the catalytic mechanism and enhance ORR performance.

Heteroatom doping in defective nanographenes has garnered significant attention, although the exact contribution of doping to the catalytic ORR activity remains debated. Heteroatoms, possessing either higher or lower electronegativity than carbon atoms, can profoundly influence the charge or spin distribution on the conjugated carbon matrix, optimizing intermediates′ adsorption energy and enhancing ORR activity. Section 5 provides a detailed discussion on this matter. In Section 3, the impact of defects, such as pentagon defects, on the charge distribution of conjugated π-electrons in graphene is explored. These defects disrupt symmetry, lowering the energy barrier for oxygen activation. Interestingly, several studies have reported that defective carbon catalysts exhibit comparable or even higher ORR activities compared to their heteroatom-doped counterparts. As a typical example, Jia et al. conducted a proof-of-concept study to establish the correlation between carbon defects and ORR performance.[77] Their results suggest that the pentagon defects are the major active sites for the enhanced acidic ORR compared to other defects. No matter whether defective carbon or doped carbon possesses higher ORR activity, it has reached a consensus that integrating these two active sites into one catalyst can achieve the best ORR performance.[111–112] Chai et al. presented a general consideration of possible ORR mechanisms for various structures in nitrogen-doped carbon alloy catalysts (CACs) based on first-principles calculations.[111] Theoretical results indicated that a particular structure of a nitrogen pair doped Stone–Wales defect, achieved by tunning the curvature around the active site, provides a good active site with a limiting potential approaching the maximum limiting potential (0.80 V) in the

volcano plot for the ORR activity of CACs. Li et al. reported the integrity of three kinds of active sites, including edged thiophene S, graphitic N, and pentagon defects, in one catalyst by N-modified S defects in carbon aerogel (denoted as NSCA).[112] This metal-free material exhibited outstanding oxygen reduction reaction (ORR) activity in both acidic and alkaline electrolytes (half-wave potentials of 0.76 V in 0.5 M H_2SO_4 and 0.1 M $HClO_4$; 0.85 V in 0.1 M KOH). The same group used computational simulations to probe the role of heteroatoms in graphene with the pentagonal carbon (C5) defect as model ORR catalysts.[113] They calculated 14 stable models of the single and dual heteroatom-modified C5 defect by DFT analysis as shown in Figure 11a. The calculated overpotentials of the most active atoms in each model are presented in Figure 11b. It can be seen that the NS–G shows much higher overpotential than that of the pure C5 defect (1.21 V versus 0.70 V), indicating that the pure C5 defect is more active than heteroatoms for the acidic ORR, which is consistent with our previous study. When C5 is co-modified by N and S (C5+N+S), it exhibits the lowest overpotential among all of the established models. It is suggested that defects are essential for catalyzing the ORR, and dopants are favorable for promoting the activity of defects. The single heteroatoms S, N, and P, but not B, are beneficial for tuning the electronic structures of the C5 defect to improve the ORR activity.

It is recognized that the same dopant within the carbon network can manifest in several configurations, complicating the identification of genuine ORR active sites for individual doped carbon catalysts. It is natural to infer that the synergistic interaction between dopants and defects can further complicate the active site identification. For example, Wang et al. reported that pyridinic N-dominated doped graphene with abundant vacancy defects exhibited ORR activity with a half-wave potential of 0.85 V in alkaline.[114] DFT analyzed seven types of pyridinic-N configurations (i.e., 1 N, 2 N, 3 N-1, 3 N-2, 4 N, 5 N, and 6 N) at the edge of the vacancy defect in the graphene model as shown in Figure 11c. It was found that the 4 N (quadri-pyridinic N) configuration exhibited the best OER performance due to the lowest overpotential of 0.28 V (Figure 11d). Liu et al. constructed graphitic-nitrogen (GN)-bonded pentagons in graphitic carbon to improve the intrinsic activity of the carbon sites and increase the number of active sites via expanding the interlayer spacing.[115] The atomic-level structure of as-formed GN-bonded pentagons was characterized by X-ray absorption spectroscopy and aberration-corrected electron microscopy. They used a catalytically active armchair-edge pentagon and calculated the possible N-substituted carbon atoms adjacent to the catalytic site. The pentagon after N-doping at site-x is named as P–Nx, for instance, the site-4 being substituted by nitrogen (blue ball in Figure 11e) is labeled as P–N4. The theoretical onset potential significantly improves from 0.45 V for a pentagon-defective site to 0.79 V for the P–N4 and P–N5 (Figure 11f), which are close to that of Pt with 0.8–0.9 V. It should be

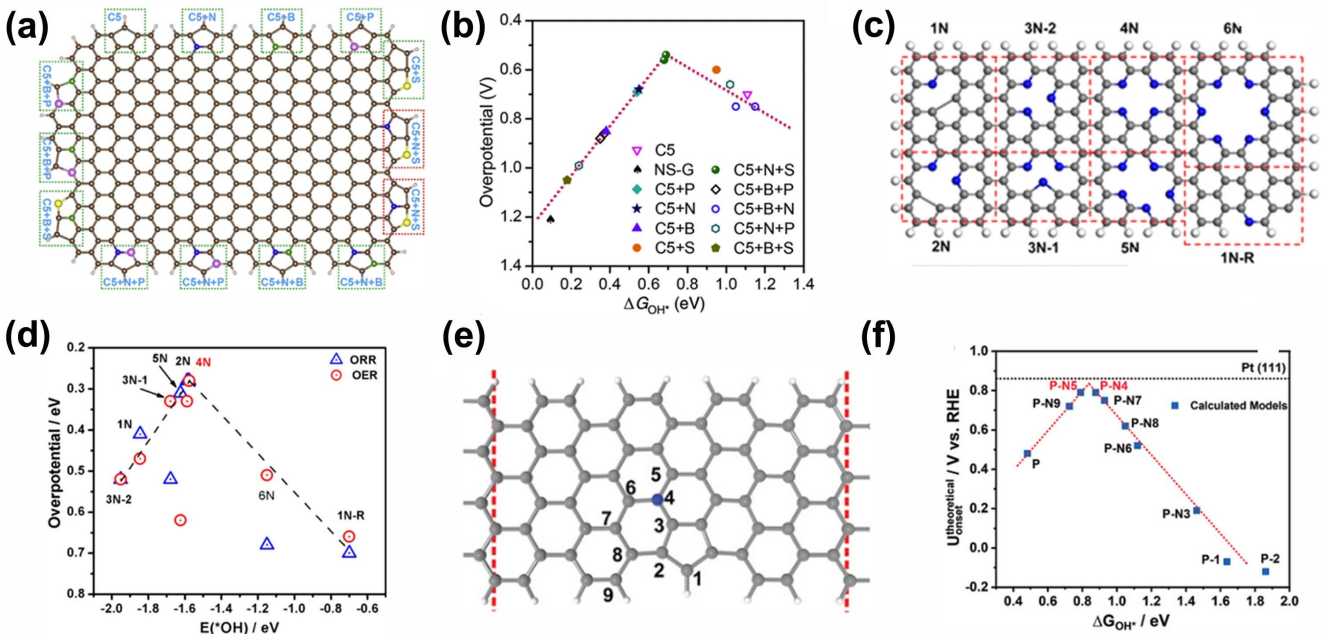

Figure 11. (a) Schematic summary of the proposed 14 configurations of the single and dual heteroatom-tuned C5 defect; brown, blue, green, pink, and yellow represent C, N, B, P, and S atoms, respectively and (b) ORR volcano plot of overpotential versus adsorption energy of OH , indicating the C5+N+S as the optimal active site for the acidic ORR. (reproduced with permission from,[113] copyright 2020, Elsevier). (c) Seven types of pyridinic-N-contained sites (1 N, 2 N, 3 N-1, 3 N-2, 4 N, 5 N, and 6 N) in the graphene model and (d) corresponding overpotential versus adsorption energy of *OH along the ORR and OER pathways without considering the effect of pH. (Reproduced with permission from,[114] copyright 2018, American Chemical Society). (e) Nitrogen-doped topological structure model, the one nitrogen-substituted site in the pentagon structure is labeled with numbers 1–8, respectively. The blue ball represents a nitrogen atom and (f) The theoretical ORR onset potential versus adsorption energy of OH*. (Reproduced with permission from,[115] copyright 2021, WILEY-VCH Verlag GmbH & Co. KGaA, Weinheim).

noted that the N-substituted site-9 is a pyridinic-N dopant and its activity is lower than the graphitic-N dopant for P–N4 and P–N5. As discussed in previous sections, The electrochemical method through the two-electron ORR emerges as an alternative and green route to H_2O_2 production. This can also be achieved by tuning the ORR pathway via modulating the cooperation between dopants and defects in carbon catalysts. Hertor et al. used theoretical and experimental methods to reveal the mechanism involved in the ORR on nitrogen-doped graphitic carbon materials.[116] An atomistic step-by-step ORR mechanism is proposed to understand the selectivity of the reaction toward the four-electron and two-electron processes. The results show that graphitic N sites favor the two-electron pathway, similar to three pyridinic N sites. Meanwhile, the one or two pyridinic N sites lead to the four-electron pathway. The calculations show the importance of dangling bonds and/or pentagonal C rings in selectivity toward the four-electron pathway. While Zhang et al. designed and synthesized a pentagonal defect-rich nitrogen-doped carbon nanomaterial (PD/N–C) by creatively using fullerene (C_{60}) as the precursor subject to ammonia treatment.[117] It achieves outstanding ORR activity, $2e^-$-selectivity, and stability in acidic electrolytes, surpassing the benchmark $PtHg_4$ alloy catalyst. The flow cell based on the PD/N–C catalyst achieves nearly 100 % Faraday efficiency with a remarkable H_2O_2 yield. Experimental and theoretical results reveal that such superb two-electron ORR performance of PD/N–C originates from the synergism between pentagonal defects and nitrogen dopants.

The synergy between size effect and heteroatom doping in nanographenes catalysts promises enhanced ORR activity, primarily by capitalizing on the increased density of active edge sites in smaller-sized graphene, facilitating better accommodation of dopants. For instance, Li et al. achieved this synergy by preparing uniform N-doped graphene quantum dots (N-GQDs) with diameters ranging from 2 to 5 nm and a N/C atomic ratio of 4.28 % (Figure 12a–b) using N-containing tetrabutylammonium perchlorate (TBAP) in acetonitrile as the electrolyte.[85] Electrochemical tests demonstrated a well-defined cathodic peak in cyclic voltammetry (CV) curves (Figure 12c) in O_2-saturated but not N_2-saturated KOH solution for N-GQDs/graphene. The ORR onset potential was approximately −0.16 V with a reduction peak at around −0.27 V, comparable to commercial Pt/C catalyst. Unlike Pt/C, the N-GQD/graphene electrode exhibited stable ORR activity in methanol-containing electrolyte, indicating remarkable tolerance to crossover effects. The reduction in graphene size exposes more edge sites, providing more energetically favorable sites for nitrogen dopants, as suggested by theoretical calculations.[119] Hence, extensive efforts have focused on maximizing edge site density in carbon matrices and introducing dopants either in situ during edge exposure or via post-treatment. Jeon et al. produced edge-selectively sulfurized graphene nanoplatelets (SGnP) through ball-milling pristine graphite with sulfur (S_8).[43] The C–C bond breaking of graphitic frameworks and delamination of graphitic layers upon ball-milling lead to the drastically reduced grain size of graphite and generate active carbon species (carboradicals, carbocations, and carbanions) to pick up sulfur to yield SGnP, as shown in Figure 12d. TEM image showed SGnP with a highly ordered structure, with a honeycomb lattice in the basal area and some distortion at the edge region (arrow, Figure 12e). The resulting SGnP exhibited a significantly improved ORR onset potential of approximately −0.22 V compared to pristine graphite (−0.40 V), with a limiting current approaching 93.4 % of commercial Pt/C (Figure 12f). Direct experimental evidence from Yang et al. confirmed the pivotal role of edge sites in ORR performance by implementing edge engineering in nanocarbons with controllable edging degrees.[118] They unzipped the outer walls of multi-walled carbon nanotubes (MWCNTs) using an oxidative process, exposing variable edge contents (Figure 12g). The ORR activity was found to correlate positively with edge content until a critical point where decreased conductivity impeded electron transfer, thus diminishing ORR performance. Incorporating heteroatoms into these unzipped MWCNTs further underscored the importance of edge sites in heteroatom doping, revealing a positive correlation between incorporated heteroatom content and edging level. This synergy between active edge sites and edge-favored doping culminated in the development of N and S co-doped graphene nanoribbons with a four-electron-dominated ORR pathway, superior long-term stability, and enhanced tolerance to methanol crossover effects compared to commercial Pt/C (20 wt %) catalysts.

7. Conclusions

The exploration of advanced nanographenes-based ORR catalysts is of great significance for the development of future clean energy.[23] Understanding how the physical (defects/size) and chemical structure (heteroatom-doping) of nanographenes materials affect their electronic properties and intrinsic reactivity offers new opportunities for researchers to harness the full potential of nanographenes in enhancing ORR process.[29] This paper provides a comprehensive review of the important roles that defects, size, and dopants play in enhanced ORR electrocatalysis, an important process for PEMFCs and MABs technologies. Although the detailed mechanisms and influence involving different functionalized nanographenes are still yet to be further understood with some confusing and ambiguous points, recent progress suggests some key insights for consideration that could improve ORR performance based on defects effect, size effect and doping effects: Nanographenes's ORR activity is significantly enhanced through chemical doping, which alters local charge distribution and improves O_2 adsorption, turning carbon and dopant atoms into active catalytic sites.[15] Edge modifications, such as sulfur-doped O=S=O groups, further enhance adsorption and catalytic activity. [26] Multiple-atom doping has consistently outperformed single-element doping, revealing synergistic effects that boost ORR performance while providing a low-cost strategy for improved catalysis.[26] In addition, nanographenes's large surface area allows for abundant active sites and

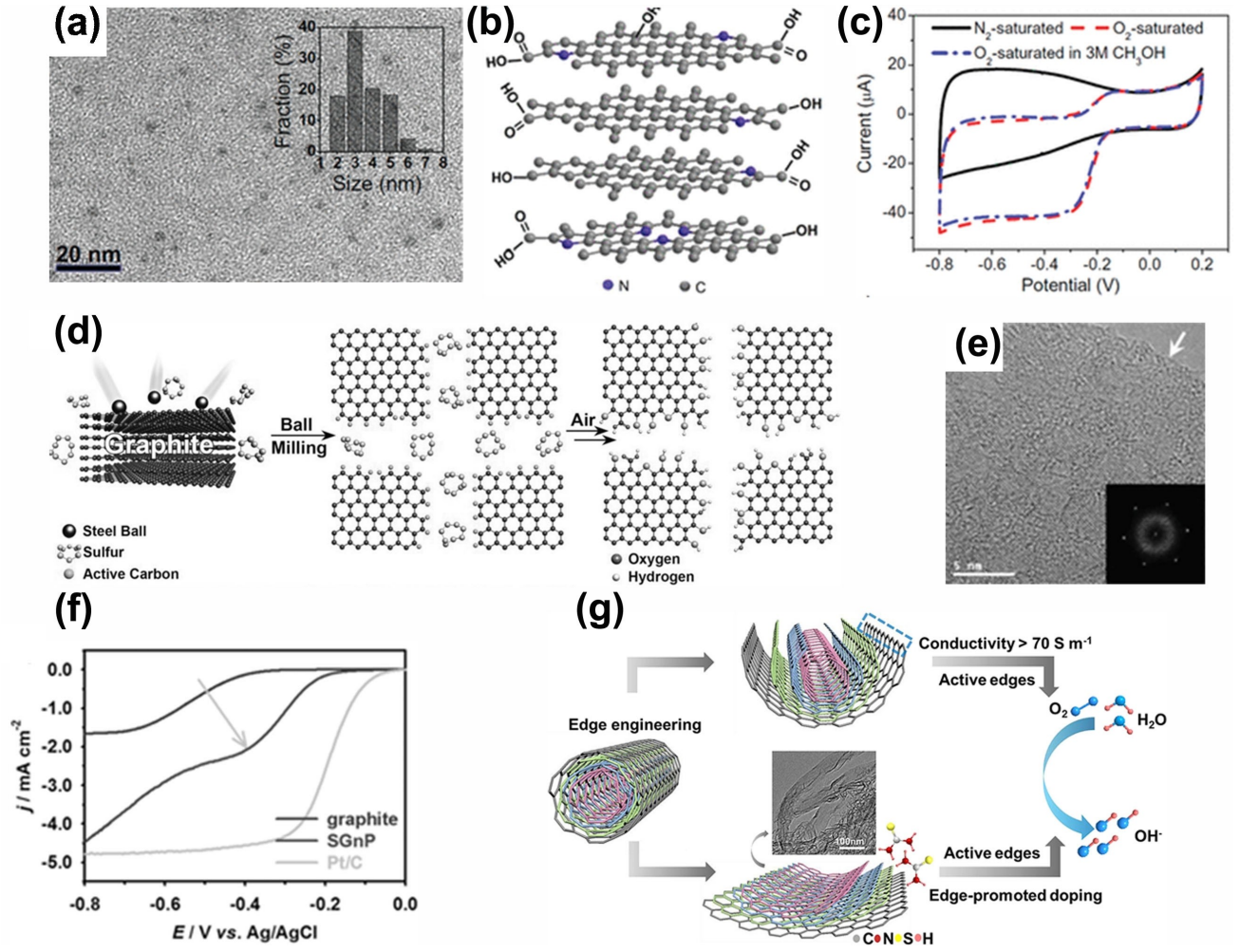

Figure 12. (a) TEM image, (b) possible structure for as-prepared N-GQDs and (c) CVs of N-GQD/graphene on a GC electrode in N_2-saturated 0.1 M KOH, O_2-saturated 0.1 M KOH, and O_2-saturated 3 M CH_3OH solutions. (Reproduced with permission from,[85] copyright 2012, American Chemical Society). (d) A schematic representation of the ball-milling process for the synthesis of SGnP, (e) TEM image of SGnP; the insets are selected area diffraction (SAED) patterns and (f) Linear sweep voltammograms of the sample electrodes in an O_2-saturated 0.1 M KOH solution at a scan rate of 10 mV s^{-1} with a rotation rate of 1600 rpm. (Reproduced with permission from,[43] copyright 2013, WILEY-VCH Verlag GmbH & Co. KGaA, Weinheim). (g) A scheme for the preparation of unzipped MWCNTs with controllable edge content. (Reproduced with permission from,[118] copyright 2019, Elsevier).

prevents atom aggregation, while its high electrical conductivity speeds up electron transfer, enhancing reaction kinetics.[120] Furthermore, defects like zigzag and pentagon edges, as well as wrinkles and vacancies, play a crucial role in boosting ORR activity.[14, 25] Targeted creation of these defects is key to improving ORR performance. Moreover, nanographenes's size also affects ORR, with smaller and thinner sheets providing more edge sites, further boosting ORR activity. Therefore, precise control over size during synthesis, along with theoretical models, serves as the main role in ORR optimization.[46, 80] Besides that, size, defects, and doping often work synergistically, enhancing ORR by altering surface charge and electronic structures, making the development of strategies to exploit these effects essential for high-performance ORR catalysts.[65] The different configurations of dopants, size, and defects contribute discriminatively to the electronic structure deformation, and therefore distinct catalytic activities.

Although it is exciting to find a way to make use of synergistic effect endowed by dopants, size, and defects, some significant challenges still exist, which should draw our further attention to exploring the highly efficient nanographenes-based ORR electrocatalysts:[121]

1. Although heteroatoms-doped graphene has been typically used as ORR catalysts, certain drawbacks, such as the expensive, toxic, and corrosive behavior of the precursor materials and complex template utilization, limited their large-scale production. If the naturally accessible biomass waste consisting of carbon and needed doping elements could be directly exploited as a synthetic precursor, the aforementioned limitations could be somehow resolved. Thus, a necessary focus has to be taken into account to deploy environmentally friendly and

sustainable starting resources for the heteroatoms doped graphene toward enhanced ORR kinetics. Meanwhile, it is still tough to control the doping concentration, doping, bonding formats, and distributional uniformity of all these synthetic methods. This is especially specific to the cases of co-doping. All of these factors directly or indirectly determine the kinetics of the doped graphene in ORR. Therefore, the development of better synthetic strategies towards controllable and targeted preparation is still much needed.[121–122]

2. The nature of electrocatalytically active sites facilitating ORR and the origin of catalytic reactivity when it happens to various dopants or defects are still controversial. It is still difficult to accurately synthesize graphene containing a single defect or defect-free heteroatom-doped graphene. Therefore, the investigation of their conformational relationships is still not precise enough. In this regard, the development of precise synthesis strategies to produce single-defect/doped graphene is essential to understanding the ORR activity of graphene and thus promotes the further enhancement of the ORR activity of graphene.[121–122]
3. Regarding defect-rich nanographenes, the specific defect species need to be identified when we talk about the impact of the defect effect on ORR performance. Advanced electron microscopy and spectroscopy techniques have successfully revealed the presence of intrinsic carbon defects and the overall defect degree of functionalized graphene in previous research. The improvement strategy for the electrocatalytic activity of ORR is to increase the content of targeted intrinsic defects and density of defectiveness that are extensively recognized to possess theoretical activity based on DFT calculation results. However, it is noted that the measurement of the density of specific topological defects in the graphene matrix and the corresponding ratio between these defects and conventional hexagonal carbon rings is hardly available.[15, 123]
4. It is well-known that the sizes of catalysts can strongly influence the catalytic efficiency, namely the nanometer size effect. For nanographenes, their size can be diverse according to their synthetic technique, determining their electrocatalytic ORR performance. The previous research mainly focuses on disclosing the relationship between size effect and reaction activity in the lateral and thickness directions. By optimizing the sizes in the lateral direction, the nanographenes could expose abundant edge sites with quantum confinement effects, thus boosting ORR performance. Besides, the thin nanographenes possess more edge sites, which can promote the electron transfer for ORR. To further disclose the size effect, much effort has been made to precisely control nanographene size via top-down and bottom-up approaches. The combination of experimental and theoretical investigation can largely promote the revelation of the size effect of nanographenes for electrolytic ORR. However, the controllable fabrication of nanographenes of a certain size still remains a challenge. Advanced architectural techniques for tailoring graphene and bottom-up synthesis need to be developed. Besides, the present theoretical investigations are limited to the models of dozens of atoms, which cannot represent all the properties of nanographenes, thus lacking the accuracy of the size effect investigation. Therefore, more precise theoretical methods should be put forward. More importantly, the size effect investigations of nanographenes are imposed by the lesser conjunction of experimental and theoretical observations, which should be further resolved.[124]
5. In most instances, as aforementioned information, nanographenes with the combination of heteroatom dopants, applicable size and various tuned defects could generate the best ORR activities. However, the mechanism of how they interact with each other and co-engineer the ORR performance has not been fully understood. Normally, the theoretical calculation by DFT is employed to display the correlation with the electronic structure, intermediate properties, and electrocatalytic activity. However, there is a massive gap between the practical situations and the results from modeling. Therefore, it is necessary to combine with more powerful in situ or operando techniques to observe the real-time process during ORR electrocatalysis, which will be very useful to further understand the synergistic effect serving as the origin of boosted ORR activity.[125]
6. The stability of carbon materials in oxygen electrocatalytic systems has been a major obstacle to their industrialization. The vast majority of current work focuses more on the enhancement of ORR activity of graphene by defects, doping, and size, while the effects of these factors on stability have been neglected. Usually, catalysts with high activity exhibit insufficient operating stability. The relationship between activity and stability needs to be balanced when optimizing graphene coordination structures.[126]
7. Although the reduced graphene oxide sheets were widely used to load single atoms, their physical chemical properties are inferior due to their structural defects compared with pure graphene.[120] It is difficult to fabricate graphene oxide or reduced graphene oxide with controllable size and specific surface to well-dispersedly anchor single atoms.[21] Moreover, the chemical morphology and orientation of graphene-based single atom should not be overlooked to improve the ORR performance.[127]

To sum up, with the contributions of the present achievements and continuous research in this field, the application of nanographenes towards the ORR is certainly a promising hotpoint in the future. Also, we hope that this review can inspire the researchers to figure out how to further improve the performance of graphene-based ORR catalysts and promote the application of nanocarbon materials in various energy-conversion technologies and electrochemical process.

Acknowledgements

This work was funded by the Volkswagen Foundation (Freigeist Fellowship No. 89592). This work was also supported by the National Natural Science Foundation of China (Grant Nos. 51902238 and Nos. 52402053), the Fundamental Research Funds for the Central Universities (WUT: 2020IVA069), China Postdoctoral Science Foundation-funded project (2020 M670343), and the Australian Research Council (DE220100746), the National Research Foundation, Singapore, and A*STAR (Agency for Science Technology and Research) under its LCER Phase 2 Programme Hydrogen & Emerging Technologies FI, Directed Hydrogen Programme (Award No. U2305D4003).

Conflict of Interest

The authors declare no conflict of interest.

Keywords: Dopants · Size · Defects · Graphene · ORR

[1] J. Zhu, S. Mu, *Adv. Funct. Mater.* **2020**, *30*, 2001097.
[2] J. Zhang, J. Zhang, F. He, Y. Chen, J. Zhu, D. Wang, S. Mu, H. Y. Yang, *Nano-Micro Lett.* **2021**, *13*, 65.
[3] Y. Shao, Z. Jiang, Q. Zhang, J. Guan, *ChemSusChem* **2019**, *12*, 2133–2146.
[4] Y. Wei, M. Zheng, W. Zhu, H. Pang, *Carbon Neutralization* **2023**, *2*, 271–299.
[5] D. Higgins, P. Zamani, A. Yu, Z. Chen, *Energy Environ. Sci.* **2016**, *9*, 357–390.
[6] R. Ma, K. Wang, C. Li, C. Wang, A. Habibi-Yangjeh, G. Shan, *Nanoscale Adv.* **2022**, *4*, 4197–4209.
[7] L. Lin, N. Miao, G. G. Wallace, J. Chen, D. A. Allwood, *Adv. Energy Mater.* **2021**, *11*, 2100695.
[8] C. Hu, L. Dai, *Angew. Chem. Int. Ed.* **2016**, *55*, 11736–11758.
[9] P. Rao, Y. Yu, S. Wang, Y. Zhou, X. Wu, K. Li, A. Qi, P. Deng, Y. Cheng, J. Li, Z. Miao, X. Tian, *Exploration* **2024**, *4*, 20230034.
[10] W. Deng, Z. Song, M. Jing, T. Wu, W. Li, G. Zou, *Carbon Neutralization* **2024**, *3*, 501–532.
[11] J. Kundu, T. Kwon, K. Lee, S.-I. Choi, *Exploration* **2024**, *4*, 20220174.
[12] D. Geng, N. Ding, T. S. Andy Hor, Z. Liu, X. Sun, Y. Zong, *J. Mater. Chem. A* **2015**, *3*, 1795–1810.
[13] C. Tang, Q. Zhang, *Adv. Mater.* **2017**, *29*, 1604103.
[14] C. Tang, H.-F. Wang, X. Chen, B.-Q. Li, T.-Z. Hou, B. Zhang, Q. Zhang, M.-M. Titirici, F. Wei, *Adv. Mater.* **2016**, *28*, 6845–6851.
[15] X. Zhang, J. Gao, Y. Xiao, J. Wang, G. Sun, Y. Zhao, L. Qu, *Chem. Asian J.* **2020**, *15*, 2271–2281.
[16] M. Li, B. Yin, C. Gao, J. Guo, C. Zhao, C. Jia, X. Guo, *Exploration* **2023**, *3*, 20210233.
[17] R. María Girón, J. Marco-Martínez, S. Bellani, A. Insuasty, H. Comas Rojas, G. Tullii, M. R. Antognazza, S. Filippone, N. Martín, *J. Mater. Chem. A* **2016**, *4*, 14284–14290.
[18] K. Waki, R. A. Wong, H. S. Oktaviano, T. Fujio, T. Nagai, K. Kimoto, K. Yamada, *Energy Environ. Sci.* **2014**, *7*, 1950–1958.
[19] X. Wang, R. K. M. Raghupathy, C. J. Querebillo, Z. Liao, D. Li, K. Lin, M. Hantusch, Z. Sofer, B. Li, E. Zschech, I. M. Weidinger, T. D. Kühne, H. Mirhosseini, M. Yu, X. Feng, *Adv. Mater.* **2021**, *33*, 2008752.
[20] Z.-Q. Wang, T.-Y. Lü, H.-Q. Wang, Y. P. Feng, J.-C. Zheng, *Frontiers of Physics* **2019**, *14*, 33403.
[21] Y. Wang, X. Zheng, D. Wang, *Nano Res.* **2022**, *15*, 1730–1752.
[22] L. Wang, A. Ambrosi, M. Pumera, *Angew. Chem. Int. Ed.* **2013**, *52*, 13818–13821.
[23] C. Zhu, S. Dong, *Nanoscale* **2013**, *5*, 1753–1767.
[24] L. Lai, J. R. Potts, D. Zhan, L. Wang, C. K. Poh, C. Tang, H. Gong, Z. Shen, J. Lin, R. S. Ruoff, *Energy Environ. Sci.* **2012**, *5*, 7936–7942.
[25] Z. Komeily-Nia, L.-T. Qu, J.-L. Li, *Small Science* **2021**, *1*, 2000026.
[26] X.-K. Kong, C.-L. Chen, Q.-W. Chen, *Chem. Soc. Rev.* **2014**, *43*, 2841–2857.
[27] K. Waki, R. A. Wong, H. S. Oktaviano, T. Fujio, T. Nagai, K. Kimoto, K. Yamada, *Energy Environ. Sci.* **2014**, *7*, 1950–1958.
[28] M. D. Bhatt, H. Kim, G. Kim, *RSC Adv.* **2022**, *12*, 21520–21547.
[29] Y. Jia, J. Chen, X. Yao, *Mater. Chem. Front.* **2018**, *2*, 1250–1268.
[30] D.-W. Wang, D. Su, *Energy Environ. Sci.* **2014**, *7*, 576–591.
[31] S. Wang, H. Jiang, L. Song, *Batteries & Supercaps* **2019**, *2*, 509–523.
[32] W. J. Lee, J. Lim, S. O. Kim, *Small Methods* **2017**, *1*, 1600014.
[33] D. Deng, L. Yu, X. Pan, S. Wang, X. Chen, P. Hu, L. Sun, X. Bao, *Chem. Commun.* **2011**, *47*, 10016–10018.
[34] Q. Li, S. Zhang, L. Dai, L. Li, *J. Am. Chem. Soc.* **2012**, *134*, 18932–18935.
[35] P. Zhang, Q. Hu, X. Yang, X. Hou, J. Mi, L. Liu, M. Dong, *RSC Adv.* **2018**, *8*, 531–536.
[36] L. Jiang, B. van Dijk, L. Wu, C. Maheu, J. P. Hofmann, V. Tudor, M. T. M. Koper, D. G. H. Hetterscheid, G. F. Schneider, *ACS Catal.* **2022**, *12*, 173–182.
[37] J. M. Chabu, L. Wang, F.-Y. Tang, K. Zeng, J. Sheng, M. D. Walle, L. Deng, Y.-N. Liu, *ChemElectroChem* **2017**, *4*, 1885–1890.
[38] X. Zhang, Z. Lu, Z. Fu, Y. Tang, D. Ma, Z. Yang, *J. Power Sources* **2015**, *276*, 222–229.
[39] D. San Roman, D. Krishnamurthy, R. Garg, H. Hafiz, M. Lamparski, N. T. Nuhfer, V. Meunier, V. Viswanathan, T. Cohen-Karni, *ACS Catal.* **2020**, *10*, 1993–2008.
[40] W. Peng, J. Liu, X. Liu, L. Wang, L. Yin, H. Tan, F. Hou, J. Liang, *Nat. Commun.* **2023**, *14*, 4430.
[41] L. Han, Y. Sun, S. Li, C. Cheng, C. E. Halbig, P. Feicht, J. L. Hübner, P. Strasser, S. Eigler, *ACS Catal.* **2019**, *9*, 1283–1288.
[42] Z. Zhuang, Y. Li, Y. Li, J. Huang, B. Wei, R. Sun, Y. Ren, J. Ding, J. Zhu, Z. Lang, L. V. Moskaleva, C. He, Y. Wang, Z. Wang, D. Wang, Y. Li, *Energy Environ. Sci.* **2021**, *14*, 1016–1028.
[43] I.-Y. Jeon, S. Zhang, L. Zhang, H.-J. Choi, J.-M. Seo, Z. Xia, L. Dai, J.-B. Baek, *Adv. Mater.* **2013**, *25*, 6138–6145.
[44] L. Tao, Q. Wang, S. Dou, Z. Ma, J. Huo, S. Wang, L. Dai, *Chem. Commun.* **2016**, *52*, 2764–2767.
[45] C. H. Choi, H.-K. Lim, M. W. Chung, J. C. Park, H. Shin, H. Kim, S. I. Woo, *J. Am. Chem. Soc.* **2014**, *136*, 9070–9077.
[46] H. Matsuyama, J. Nakamura, *ACS Omega* **2022**, *7*, 3093–3098.
[47] J. Benson, Q. Xu, P. Wang, Y. Shen, L. Sun, T. Wang, M. Li, P. Papakonstantinou, *ACS Appl. Mater. Interfaces* **2014**, *6*, 19726–19736.
[48] L. Dai, Y. Xue, L. Qu, H.-J. Choi, J.-B. Baek, *Chem. Rev.* **2015**, *115*, 4823–4892.
[49] Y. Jia, L. Zhang, A. Du, G. Gao, J. Chen, X. Yan, C. L. Brown, X. Yao, *Adv. Mater.* **2016**, *28*, 9532–9538.
[50] X. Zhao, X. Zou, X. Yan, C. L. Brown, Z. Chen, G. Zhu, X. Yao, *Inorg. Chem. Front.* **2016**, *3*, 417–421.
[51] J. He, Y. Zou, S. Wang, *Dalton Trans.* **2019**, *48*, 15–20.

[52] K. S. Novoselov, A. K. Geim, S. V. Morozov, D. Jiang, Y. Zhang, S. V. Dubonos, I. V. Grigorieva, A. A. Firsov, *Science* **2004**, *306*, 666–669.

[53] Y. Gu, Z. Qiu, K. Müllen, *J. Am. Chem. Soc.* **2022**, *144*, 11499–11524.

[54] A. Narita, X.-Y. Wang, X. Feng, K. Müllen, *Chem. Soc. Rev.* **2015**, *44*, 6616–6643.

[55] J. Wang, X. Jin, C. Li, W. Wang, H. Wu, S. Guo, *Chem. Eng. J.* **2019**, *370*, 831–854.

[56] Q. Chen, S. Thoms, S. Stöttinger, D. Schollmeyer, K. Müllen, A. Narita, T. Basché, *J. Am. Chem. Soc.* **2019**, *141*, 16439–16449.

[57] X. Zhao, C. Lu, J. Li, C. Liu, C. Cao, T. Wu, *Carbon Letters* **2023**, *33*, 155–162.

[58] H. Jin, H. Huang, Y. He, X. Feng, S. Wang, L. Dai, J. Wang, *J. Am. Chem. Soc.* **2015**, *137*, 7588–7591.

[59] S. Eigler, M. Enzelberger-Heim, S. Grimm, P. Hofmann, W. Kroener, A. Geworski, C. Dotzer, M. Röckert, J. Xiao, C. Papp, O. Lytken, H.-P. Steinrück, P. Müller, A. Hirsch, *Adv. Mater.* **2013**, *25*, 3583–3587.

[60] Y. Kumar, S. Akula, M. K. R. Souza, G. Maia, K. Tammeveski, *Curr. Opin. Electrochem.* **2024**, *47*, 101554.

[61] P. Kamedulski, M. Skorupska, P. Binkowski, W. Arendarska, A. Ilnicka, J. P. Lukaszewicz, *Sci. Rep.* **2021**, *11*, 22054.

[62] Y. Zhang, X. Xia, B. Liu, S. Deng, D. Xie, Q. Liu, Y. Wang, J. Wu, X. Wang, J. Tu, *Adv. Energy Mater.* **2019**, *9*, 1803342.

[63] D. V. Kosynkin, A. L. Higginbotham, A. Sinitskii, J. R. Lomeda, A. Dimiev, B. K. Price, J. M. Tour, *Nature* **2009**, *458*, 872–876.

[64] L. Xue, Y. Li, X. Liu, Q. Liu, J. Shang, H. Duan, L. Dai, J. Shui, *Nat. Commun.* **2018**, *9*, 3819.

[65] X.-Y. Wang, X. Yao, A. Narita, K. Müllen, *Acc. Chem. Res.* **2019**, *52*, 2491–2505.

[66] W. Yu, L. Sisi, Y. Haiyan, L. Jie, *RSC Adv.* **2020**, *10*, 15328–15345.

[67] C. Li, Z. Chen, A. Kong, Y. Ni, F. Kong, Y. Shan, *J. Mater. Chem. A* **2018**, *6*, 4145–4151.

[68] Z. Liu, S. Fu, X. Liu, A. Narita, P. Samorì, M. Bonn, H. I. Wang, *Adv. Sci.* **2022**, *9*, 2106055.

[69] L. Lu, L. Peng, C. Zhan, W. You, S. Xiao, *J. Mater. Chem. A* **2014**, *2*, 1802–1808.

[70] K. Kawasumi, Q. Zhang, Y. Segawa, L. T. Scott, K. Itami, *Nat. Chem.* **2013**, *5*, 739–744.

[71] C. Hu, R. Paul, Q. Dai, L. Dai, *Chem. Soc. Rev.* **2021**, *50*, 11785–11843.

[72] Z. Li, Z. Zhuang, F. Lv, H. Zhu, L. Zhou, M. Luo, J. Zhu, Z. Lang, S. Feng, W. Chen, L. Mai, S. Guo, *Adv. Mater.* **2018**, *30*, 1803220.

[73] K. Choi, S. Kim, *ACS Nano* **2022**, *16*, 16394–16401.

[74] J. Zhu, J. Li, R. Lu, R. Yu, S. Zhao, C. Li, L. Lv, L. Xia, X. Chen, W. Cai, J. Meng, W. Zhang, X. Pan, X. Hong, Y. Dai, Y. Mao, J. Li, L. Zhou, G. He, Q. Pang, Y. Zhao, C. Xia, Z. Wang, L. Dai, L. Mai, *Nat. Commun.* **2023**, *14*, 4670.

[75] L. Zhang, Q. Xu, J. Niu, Z. Xia, *Phys. Chem. Chem. Phys.* **2015**, *17*, 16733–16743.

[76] Y. Jia, L. Zhang, A. Du, G. Gao, J. Chen, X. Yan, C. L. Brown, X. Yao, *Adv. Mater.* **2016**, *28*, 9532–9538.

[77] Y. Jia, L. Zhang, L. Zhuang, H. Liu, X. Yan, X. Wang, J. Liu, J. Wang, Y. Zheng, Z. Xiao, E. Taran, J. Chen, D. Yang, Z. Zhu, S. Wang, L. Dai, X. Yao, *Nature Catalysis* **2019**, *2*, 688–695.

[78] C. Tang, H.-F. Wang, X. Chen, B.-Q. Li, T.-Z. Hou, B. Zhang, Q. Zhang, M.-M. Titirici, F. Wei, *Adv. Mater.* **2016**, *28*, 6845–6851.

[79] Y. Jiang, L. Yang, T. Sun, J. Zhao, Z. Lyu, O. Zhuo, X. Wang, Q. Wu, J. Ma, Z. Hu, *ACS Catal.* **2015**, *5*, 6707–6712.

[80] G. C. Bond, *Surf. Sci.* **1985**, *156*, 966–981.

[81] M. Shao, A. Peles, K. Shoemaker, *Nano Lett.* **2011**, *11*, 3714–3719.

[82] R. Reske, H. Mistry, F. Behafarid, B. Roldan Cuenya, P. Strasser, *J. Am. Chem. Soc.* **2014**, *136*, 6978–6986.

[83] A. Shen, Y. Zou, Q. Wang, R. A. W. Dryfe, X. Huang, S. Dou, L. Dai, S. Wang, *Angew. Chem. Int. Ed.* **2014**, *53*, 10804–10808.

[84] D. Pan, J. Zhang, Z. Li, M. Wu, *Adv. Mater.* **2010**, *22*, 734–738.

[85] Y. Li, Y. Zhao, H. Cheng, Y. Hu, G. Shi, L. Dai, L. Qu, *J. Am. Chem. Soc.* **2012**, *134*, 15–18.

[86] F. Hof, M. Liu, G. Valenti, E. Picheau, F. Paolucci, A. Pénicaud, *J. Phys. Chem. C* **2019**, *123*, 20774–20780.

[87] X. Zhang, Y. Xia, C. Xia, H. Wang, *Trends Chem.* **2020**, *2*, 942–953.

[88] H. Matsuyama, A. Akaishi, J. Nakamura, *ACS Omega* **2019**, *4*, 3832–3838.

[89] K. Gong, F. Du, Z. Xia, M. Durstock, L. Dai, *Science* **2009**, *323*, 760.

[90] L. Qu, Y. Liu, J.-B. Baek, L. Dai, *ACS Nano* **2010**, *4*, 1321–1326.

[91] D. Guo, R. Shibuya, C. Akiba, S. Saji, T. Kondo, J. Nakamura, *Science* **2016**, *351*, 361.

[92] S. Maldonado, S. Morin, K. J. Stevenson, *Carbon* **2006**, *44*, 1429–1437.

[93] B. Li, X. Sun, D. Su, *Phys. Chem. Chem. Phys.* **2015**, *17*, 6691–6694.

[94] T. Wang, Z.-X. Chen, Y.-G. Chen, L.-J. Yang, X.-D. Yang, J.-Y. Ye, H.-P. Xia, Z.-Y. Zhou, S.-G. Sun, *ACS Energy Lett.* **2018**, *3*, 986–991.

[95] H. B. Yang, J. Miao, S.-F. Hung, J. Chen, H. B. Tao, X. Wang, L. Zhang, R. Chen, J. Gao, H. M. Chen, L. Dai, B. Liu, *Sci. Adv.* **2016**, *2*, e1501122.

[96] Z. Hou, X. Wang, T. Ikeda, K. Terakura, M. Oshima, M. Kakimoto, S. Miyata, *Phys. Rev. B* **2012**, *85*, 165439.

[97] W. Xia, J. Tang, J. Li, S. Zhang, K. C.-W. Wu, J. He, Y. Yamauchi, *Angew. Chem. Int. Ed.* **2019**, *58*, 13354–13359.

[98] N. Yang, X. Zheng, L. Li, J. Li, Z. Wei, *J. Phys. Chem. C* **2017**, *121*, 19321–19328.

[99] K. Lee, J. Lim, M. J. Lee, K. Ryu, H. Lee, J. Y. Kim, H. Ju, H.-S. Cho, B.-H. Kim, M. C. Hatzell, J. Kang, S. W. Lee, *Energy Environ. Sci.* **2022**, *15*, 2858–2866.

[100] Y. Xia, X. Zhao, C. Xia, Z.-Y. Wu, P. Zhu, J. Y. (Timothy) Kim, X. Bai, G. Gao, Y. Hu, J. Zhong, Y. Liu, H. Wang, *Nat. Commun.* **2021**, *12*, 4225.

[101] K. Ri, S. Pak, D. Sun, Q. Zhong, S. Yang, S. Sin, L. Wu, Y. Sun, H. Cao, C. Han, C. Xu, Y. Liu, H. He, S. Li, C. Sun, *Appl. Catal. B* **2024**, *343*, 123471.

[102] H. W. Kim, M. B. Ross, N. Kornienko, L. Zhang, J. Guo, P. Yang, B. D. McCloskey, *Nature Catalysis* **2018**, *1*, 282–290.

[103] M. Fan, Q. Yuan, Y. Zhao, Z. Wang, A. Wang, Y. Liu, K. Sun, J. Wu, L. Wang, J. Jiang, *Adv. Mater.* **2022**, *34*, 2107040.

[104] S. Wang, L. Zhang, Z. Xia, A. Roy, D. W. Chang, J.-B. Baek, L. Dai, *Angew. Chem. Int. Ed.* **2012**, *51*, 4209–4212.

[105] M. Fan, J. Wu, J. Yuan, L. Deng, N. Zhong, L. He, J. Cui, Z. Wang, S. K. Behera, C. Zhang, J. Lai, B. I. Jawdat, R. Vajtai, P. Deb, Y. Huang, J. Qian, J. Yang, J. M. Tour, J. Lou, C.-W. Chu, D. Sun, P. M. Ajayan, *Adv. Mater.* **2019**, *31*, 1805778.

[106] X. Zhang, X. Wen, C. Pan, X. Xiang, C. Hao, Q. Meng, Z. Q. Tian, P. K. Shen, S. P. Jiang, *Chem. Eng. J.* **2022**, *431*, 133216.

[107] Z. Wu, Y. Yu, G. Zhang, Y. Zhang, R. Guo, L. Li, Y. Zhao, Z. Wang, Y. Shen, G. Shao, *Adv. Sci.* **2022**, *9*, 2200614.

[108] X. Zhang, X. Zhang, X. Xiang, C. Pan, Q. Meng, C. Hao, Z. Qun Tian, P. Kang Shen, S. Ping Jiang, *ChemElectroChem* **2021**, *8*, 3262–3272.

[109] Y. Wang, N. Xu, R. He, L. Peng, D. Cai, J. Qiao, *Appl. Catal. B* **2021**, *285*, 119811.

[110] J. Zhang, L. Dai, *Angew. Chem. Int. Ed.* **2016**, *55*, 13296–13300.
[111] G.-L. Chai, Z. Hou, D.-J. Shu, T. Ikeda, K. Terakura, *J. Am. Chem. Soc.* **2014**, *136*, 13629–13640.
[112] D. Li, Y. Jia, G. Chang, J. Chen, H. Liu, J. Wang, Y. Hu, Y. Xia, D. Yang, X. Yao, *Chem* **2018**, *4*, 2345–2356.
[113] X. Yan, H. Liu, Y. Jia, L. Zhang, W. Xu, X. Wang, J. Chen, D. Yang, X. Yao, *Cell Reports Physical Science* **2020**, *1*, DOI: 10.1016/j.xcrp.2020.100083.
[114] Q. Wang, Y. Ji, Y. Lei, Y. Wang, Y. Wang, Y. Li, S. Wang, *ACS Energy Lett.* **2018**, *3*, 1183–1191.
[115] S. Liu, Y. Zhang, B. Ge, F. Zheng, N. Zhang, M. Zuo, Y. Yang, Q. Chen, *Adv. Mater.* **2021**, *33*, 2103133.
[116] H. N. Fernandez-Escamilla, J. Guerrero-Sanchez, E. Contreras, J. M. Ruiz-Marizcal, G. Alonso-Nunez, O. E. Contreras, R. M. Felix-Navarro, J. M. Romo-Herrera, N. Takeuchi, *Adv. Energy Mater.* **2021**, *11*, 2002459.
[117] C. Zhang, W. Shen, K. Guo, M. Xiong, J. Zhang, X. Lu, *J. Am. Chem. Soc.* **2023**, *145*, 11589–11598.
[118] Q. Yang, Z. Xiao, D. Kong, T. Zhang, X. Duan, S. Zhou, Y. Niu, Y. Shen, H. Sun, S. Wang, L. Zhi, *Nano Energy* **2019**, *66*, 104096.
[119] M. Li, L. Zhang, Q. Xu, J. Niu, Z. Xia, *J. Catal.* **2014**, *314*, 66–72.
[120] L. Zhang, Y. Wang, Z. Niu, J. Chen, *Small Methods* **2019**, *3*, 1800443.
[121] M. V. Kannan, G. Gnana kumar, *Biosens. Bioelectron.* **2016**, *77*, 1208–1220.
[122] X. Tong, Q. Wei, X. Zhan, G. Zhang, S. Sun, *Catalysts* **2017**, *7*, DOI:10.3390/catal7010001.
[123] S. A. Samad, Z. Fang, P. Shi, J. Zhu, C. Lu, Y. Su, X. Zhuang, *2D Mater.* **2023**, *10*, 022001.
[124] T. J. Bandosz, *Carbon* **2022**, *188*, 289–304.
[125] S. Chandrasekaran, D. Ma, Y. Ge, L. Deng, C. Bowen, J. Roscow, Y. Zhang, Z. Lin, R. D. K. Misra, J. Li, P. Zhang, H. Zhang, *Nano Energy* **2020**, *77*, 105080.
[126] M. Reda, H. A. Hansen, T. Vegge, *Catal. Today* **2018**, *312*, 118–125.
[127] C. Zhu, J. Yang, J. Zhang, X. Wang, Y. Gao, D. Wang, H. Pan, *Interdisciplinary Materials* **2024**, *3*, 74–86.

Manuscript received: August 7, 2024
Accepted manuscript online: November 12, 2024
Version of record online: December 4, 2024